Passive Three Dimensional Face Recognition Using Iso-Geodesic Contours and Procrustes Analysis

Sina Jahanbin · Rana Jahanbin · Alan C. Bovik

Abstract We introduce a new model for personal recognition based on the 3-D geometry of the face. The model is designed for application scenarios where the acquisition conditions constrain the facial position. The 3-D structure of a facial surface is compactly represented by sets of contours (facial contours) extracted around automatically pinpointed nose tip and inner eye corners. The metric used to decide whether a point on the face belongs to a facial contour is its geodesic distance from a given landmark. Iso-geodesic contours are inherently robust to head pose variations, including in-depth rotations of the face. Since these contours are extracted from rigid parts of the face, the resulting recognition algorithms are insensitive to changes in facial expressions. The facial contours are encoded using innovative pose invariant features, including Procrustean distances defined on pose-invariant curves. The extracted features are combined in a hierarchical manner to create three parallel face recognizers. Inspired by the effectiveness of region ensembles approaches, the three recognizers constructed around the nose tip and inner corners of the eyes are fused both at the feature-level and the match score-level to create a unified face recognition algorithm with boosted performance. The performances of the proposed algorithms are evaluated and compared with other algorithms from the literature on a large public database appropriate for the assumed constrained application scenario.

1 Introduction

Biometrics, which refers to automatic identification of individuals based on their measurable physiological or behavioral attributes, has received considerable attention from academia, government agencies, and industries to the extent that several degree programs focusing on the engineering and design of biometric systems (Bachelor of Science in Biometric Systems, West Virginia University. http://www.lcsee.cemr.wvu.edu/ugrad/degree-info.php?degree=bsbs) have been established. This interest which is fueled by the emergence of important applications (e.g. access control to facilities, surveillance, and airport screening) has taken on a new urgency in light of heightened global security concerns and a desire to constrain the mobility of criminals (Morgan and Krouse 2005; Latta 2004).

Although many biometric modalities (face, fingerprints, iris, hand geometry, gait) have been considered over the last few decades, no single modality outperforms others in all applications and deployment conditions. For example, fingerprints are not suitable for an access control to a coal mine where users are likely to have dirty and worn fingerprints (Biometrics frequently asked questions 2006). Because of its unique advantages, the human face is considered the modality of choice in many sensitive applications. For example, the International Civil Aviation Organization mandated the use of face in its 2002 resolution (ICAO 2004) as the primary biometric modality in the new generation

S. Jahanbin (✉)
KLA-Tencor Corp., Milpitas, CA 95035-7916, USA
e-mail: sina.jahanbin@utexas.edu

R. Jahanbin
Harmonic Inc., San Jose, CA 95134, USA
e-mail: rana_jahanbin@alumni.utexas.net

A. C. Bovik
The Department of Electrical and Computer Engineering,
The University of Texas at Austin, Austin, TX 78712, USA
e-mail: bovik@ece.utexas.edu

of travel documents. Facial images are easily acquired with ordinary cameras with minimum cooperation from subjects. Acquisition of facial images is contact-less and if passive sensing is used, largely non-intrusive and does not raise health concerns, whereas fingerprint scanners requires touching a sensor used by countless individuals (Bowyer et al. 2004). Facial biometrics are understandable for human operators and the validity of the decisions made by a machine can quickly be verified by a human supervisor, unlike iris scans or fingerprints.

Here we introduce new 3-D face recognition approaches targeting specific application domains having restricted acquisition requirements. One such application of high importance for national security is airport screening, where face recognition is performed under the supervision of a human administrator. Operating under assumptions specified by the National Institute of Standards and Technology (NIST), we assume that subjects are asked to stand at a fixed distance from the camera without wearing accessories (e.g. glasses or hats) and to face the camera. Other than the above constraints, other factors such as slight head pose variations, changes in the facial expression, variation in illumination, and make-up should be taken into consideration. We demonstrate the efficiency of our model using a very large appropriate database of co-registered 2-D and 3-D face images acquired using a passive modality (i.e. optical stereo ranging).

2 Related Work

To date, the majority of implemented face recognition algorithms have been based on intensity (also known as 2-D or portrait) images. Unbiased evaluations, such as the Face Recognition Vendors test (FRVT) 2006 (Phillips et al. 2010) indicate that despite the high sophistication achieved in 2-D face recognition techniques, their collective performance remains unsatisfactory, and degrades significantly with variations in lighting, pose, makeup, or facial expression (Phillips et al. 2003). However, the emergence of reliable and inexpensive 3-D scanners has opened new opportunities for researchers to use 3-D structure of the face alone or in combination with 2-D information to attain better performance (Bowyer et al. 2006).

Many early 3-D face recognition approaches were simply extended versions of holistic 2-D approaches in which the portrait images are replaced by range images (Gupta et al. 2007). Typically, the input range images are aligned and then reformatted into a feature vector. The dimensionality of these high-dimensional feature vectors are reduced using standard statistical dimensionality reduction techniques, for instance, principle component analysis (PCA) is used in what is known as Eigensurfaces (Russ et al. 2006; Hesher 2003) and linear discriminant analysis (LDA) is used in the so called Fishersurfaces (Gokberk et al. 2005; Heseltine et al. 2004). The main drawback of holistic approaches is their sensitivity to drastic deformations (e.g. open mouth), facial expression, and improper alignment of faces (Gupta et al. 2007).

A popular trend in 3-D face recognition are direct "surface matching" techniques in which the two facial surfaces under comparison are iteratively placed as closely as possible in 3-D space by minimizing a distance metric. A well-known example of this category is the iterative closest point (ICP) algorithm in which a variant of mean squared error (MSE) or Hausdorff distance is used to compare surfaces at each stage (Lu et al. 2006; Lu and Jain 2005). Although such surface matching techniques have shown to be successful, they are computationally very expensive which is problematic when searching large databases. Another limitation of surface matching is sensitivity to facial expression and global deformations of the face.

In recent years, many of the problems associated with traditional holistic approaches have been mitigated by introducing region ensembles approaches (Queirolo et al. 2010; Faltemier et al. 2008; Kakadiaris et al. 2007; McKeon and Russ 2010; Boehnen et al. 2009) which are considered as a compromise between holistic and local face recognition approaches. In region ensembles approaches, faces are divided into multiple smaller subregions. Comparisons between two faces begin by independently comparing the corresponding subregions. Finally, the committee of similarity scores collected from various subregions are merged into a final decision. Region ensembles approaches are robust against facial expression changes and partial occlusions, and many of them are currently among the top performing algorithms.

Geodesic distance based features have been considered by researchers since new studies (Bronstein et al. 2005) suggest that the variations of geodesic distances between pairs of points on the human face are insignificant under expression variations. Gupta et al. (2010) proposed "Anthroface 3D", a face recognition algorithm based on geodesic and 3-D Euclidean distances between 10 automatically annotated fiducial points. "Anthroface 3D" is not a pure 3-D approach, since portrait clues are used to assist the fiducial detection step. Motivated by the desirable properties of geodesic distances, especially their pose invariance and robustness against changes in facial expression, we introduce geodesic distance based features extracted around a limited number of landmarks which are reliably detectable and highly descriptive. In this work, unlike the "Anthroface 3D" features that are distributed all over the face, features extracted around each fiducial point are only descriptive of the surface characteristics in the vicinity of the target landmarks. This property makes the proposed feature suitable for state-of-the-art "region ensembles approaches".

Recently, several 3-D face recognition algorithms have been proposed in which three-dimensional facial surfaces are represented by unions of curves. Comparisons between facial surfaces is conducted implicitly by comparing the corresponding contour sets. This approach is mainly motivated by the fact that curve matching is a much more studied problem than free-form surface matching, and a wealth of curve matching techniques are available (Mpiperis et al. 2007). Unlike facial surfaces, contours can be parameterized canonically and thus can be naturally compared (Samir et al. 2006). The number of data points on facial contours is only a fraction of the number of points available on the original facial surface, thus resulting in dramatical reductions in the required computation and storage. Contours are often defined using level-sets of real-valued functions such as curvature, depth, or gradient defined on facial surfaces.

Nagamine et al. (1992) used 3-D curves resulting from the intersection of the facial surface with vertical planes, horizontal planes, or cylinders as representative facial curves. The depth values are sampled along each cross-sectional curve to create a feature vector. The similarity between two facial surfaces is measured by the Euclidean distance between their feature vectors. Experimental results indicated that the vertical profile curves extracted from the central portion of the face have the strongest distinctiveness. Circular cross-sections extracted around the nose tip also demonstrated high discriminating power. The main advantage of circular curves is their robustness against rotational variations. The horizontal profiles were shown to be the least effective ones.

One of the earliest contour-based facial surface representations is the "point signature" concept proposed by Chua et al. (2000). For any given fiducial (source point) on the facial surface, a 3-D contour C is obtained by intersecting the surface with a sphere of radius R centered at that source point. A plane is fitted to the contour C, then translated to the source point in a direction normal to the plane. The point signature is a vector of signed distances sampled at regularly spaced angles between each point on C and its projection on the plane. A drawback of the point signature approach is that the neighborhood of a surface point is sometimes ambiguous (Sun and Abidi 2001). This shortcoming arises from the use of Euclidean distance. The ambiguity can result in problematic self-intersecting or discontinuous contours.

Mpiperis et al. (2007) and Samir et al. (2006) represented range images by planar level-set contours of the depth function. The comparison between two faces is performed by comparing 2-D iso-depth contours at the same depth. Three different planar contour features are investigated in Mpiperis et al. (2007): the Hu moments (Hu 1962), elliptic Fourier descriptors (Due Trier 1996), and curvature scale space (CSS) (Mokhtarian and Mackworth 1986). The performances of the proposed algorithms in Mpiperis et al. (2007) are evaluated on a database of 800 range images from 20 subjects (40 images per subject). Results are compared with a variant of point signatures (Chua et al. 2000) showing a better performance for iso-depth contour matching. One limitation of the iso-depth contours is that they are susceptible to changes in the gaze direction. Some Euclidean transformations of facial surface, such as in-depth rotation caused by inaccurate estimation of gaze direction, introduce irreversible deformations in the resulting iso-depth contours. To mitigate the effect of pose variation on recognition performance, an extremely accurate gaze alignment step is required that is costly and difficult.

Mahoor and Abdel-Mottaleb (2009) used ridge lines to represent range images in their proposed 3-D face recognition algorithm. The ridge lines are found by thresholding the maximum principle curvature, k_{max}, of the facial surface. In order to find the best match between a probe image and gallery images, an iterative approach similar to the ICP algorithm is utilized to find the optimum pose between probe and gallery ridge lines resulting in the minimum Hausdorff distance. The final Hausdorff distance is used as a measure of the difference between a probe and a gallery facial surface. One disadvantage of the ridge line representation is that the computation of curvatures involves higher order derivatives and is thus sensitive to 3-D scanner noise.

Berretti et al. (2010) proposed a 3-D face recognition algorithm in which range images are segmented into equal width iso-geodesic stripes at increasing distance from the nose tip. Next, the face is compactly represented by an attributed relational graph where each node represents a stripe, and each edge of the graph is annotated by 3-D "weighted walkthroughs" (3DWW) between two stripes. The 3DWW between each pair of stripes captures the relative spatial displacements between all pairs of points of the input stripes. Eventually, two given faces are compared by comparing their corresponding annotated graphs.

A new contour-based 3-D object representation called the "point fingerprints" (because of their similarity to fingerprint patterns) was proposed by Sun and Abidi (2001) and tested for surface registration. In this method, surfaces are represented by sets of 2-D contours that are the projection of the 3-D iso-geodesic contours on a plane tangent to the surface at the central landmark. Motivated by point fingerprints' effectiveness, we implemented a novel face recognition algorithm (Jahanbin et al. 2008) where 3-D faces were represented by planar point fingerprints extracted around the automatically pinpointed nose tip. Iso-depth contours were also extracted with respect to the nose tip and their performance in recognizing faces was considered as a benchmark for comparison. The shapes of obtained planar iso-depth and fingerprint contours were characterized by two types of attributes: radial Euclidean distances from the nose tip and a set of five commonly used shape descriptors (ratio of principal axes, convexity, compactness, cir-

cular variance, and elliptic variance) as defined in Peura and Iivarinen (1997). These features were independently tested in a face authentication experiment using both a one-nearest neighbor (1NN) classifier using the Euclidean distance metric in an LDA dimensionality reduced feature space, and a support vector machine (SVM) classifier. The results indicated that no matter what classification rule is used, facial fingerprint contours (2-D projections of iso-geodesic contours) outperform their iso-depth counterpart.

In this work, for the first time, the concept of iso-geodesic contour based surface representation is combined with statistical learning techniques and region ensemble approaches to construct a face recognition model with competitive performance and robustness against pose and facial expression variations. This model embodies several unique contributions to the fields of 3-D face recognition, 3-D surface representation, and object detection.

One important contribution is the use of unions of iso-geodesic contours extracted around automatically detected landmarks to represent the 3-D surface of the human face. This surface representation has some unique advantages that make it useful in related applications such as 3-D surface representation and 3-D object detection. Iso-geodesic contours provide a compact representation of the surface by saving only a small fraction of the surface points. Another advantage of iso-geodesic contours over other representations such as iso-depth contours in free-form surface representation is that the shapes of iso-geodesic contours do not change with Euclidean transformations of the surface such as in-depth rotations.

A second important contribution is a set of innovative pose invariant contour features, including those derived from a Procrustean curve matching procedure. The application of these novel features is not limited to face recognition applications. Unlike other 3-D contour features proposed in the literature which are extracted from the projection of 3-D contours onto 2-D planes (Samir et al. 2006; Mpiperis et al. 2007; Sun and Abidi 2001), these new features are directly extracted from 3-D contours in 3-D space. Hence, they do not compromise the iso-geodesic contours' pose invariance advantage over other contour representations, such as iso-depth contours.

The third contribution is a hierarchical scheme to statistically analyze, select, and combine discriminative features from contours around each landmark into a classifier specialized in that region. Inspired by the effectiveness of "region ensembles approaches", the proposed hierarchy combines these regional classifiers into a unified face recognition model with boosted performance. Sensitivity evaluations confirm the robustness of the proposed 3-D face recognition algorithm against facial expression variations and fiducial detection errors.

3 Present Work and Overview

As mentioned in the previous section, iso-geodesic contours have desirable properties in comparison to other contours in representing free-form surfaces. The shapes of iso-geodesic contours do not change with Euclidean transformations of the surface (head pose variations in our application) such as in-depth rotations, which greatly affect iso-depth contours. Unlike iso-Euclidean contours, self-crossings and discontinuities do not occur in iso-geodesic representations. Here, we seek new directions to improve the preliminary iso-geodesic contour-based 3-D face recognition concept (Jahanbin et al. 2008). In addition to nose tip, iso-geodesic contours are extracted from the inner eye corners as well, providing additional discriminative features, leading to improved face recognition performance. Nose tip and inner corners of the eyes are prominent fiducials which can be detected accurately. Besides, these landmarks are located on rigid yet distinctive region of the face. The shape of eye socket and nasal regions do not change as much as other regions such as mouth and cheeks with limited variations in facial expressions. Hence, features extracted from these regions are likely to be less sensitive to facial expression changes. Automatic fiducial detection and contour extraction procedures are explained in Sect. 4.

Previously in Jahanbin et al. (2008), the obtained 3-D iso-geodesic contours were projected onto a tangent plane at the nose tip, and features were indirectly calculated from the projected planar contours because planar contour features are easier to obtain. This projection step discards important elevation information as we transform a 3-D contour into a planar one. Also, determining the tangent plane at the nose tip is very noise sensitive and may be more so at inner eye corners. Inaccurate tangent plane determination results in lower quality features. In order to solve this problem, we introduce new pose invariant features, including radial distances from the origin, curvatures along the contour path, and features derived from a Procrustean curve matching procedure defined on iso-geodesic contours in 3-D space. These new features do not compromise the iso-geodesic contours' pose invariance advantage over other contour representations, such as iso-depth contours. Contour feature extraction steps are explained in Sect. 5.

In our previous work (Jahanbin et al. 2008), various features from planar contours were evaluated independently, but no effort was made to merge them into a unified face recognition system. Here, features calculated from each contour set (nasal and inner corners of the eyes contour sets) are independently evaluated and then combined hierarchically to create three parallel face recognition systems (one per fiducial). Inspired by the effectiveness of "region ensembles approaches", these three face recognizers that specialize different regions of the face are fused using both feature-level

and match score-level fusion techniques to create a unified face recognition algorithm with boosted performance. The classification task is performed by a 1NN classifier using Euclidean distance metric in LDA subspace and the results are evaluated and compared in both authentication and identification setups. The proposed algorithms deliver very promising performance and show robustness against facial landmark detection errors in sensitivity evaluation studies. Face recognition results are presented and compared with other leading algorithms from the literature on the same database in Sect. 7 followed by a discussion in Sect. 8.

4 Contour Extraction

In order to obtain facial contours from a facial range image, it is necessary to define real-valued functions on that surface (Milnor 1963). In this article, the normalized geodesic distances from three detected landmarks (nose tip, inner corners of the left and right eyes) are the real-valued functions of choice. Level-sets of each function provides closed contours around the target landmark on the facial surface. In the following subsections, the dataset used for experiments in this article is introduced followed by an explanation of the automatic fiducial point detection and iso-geodesic contour extraction steps.

4.1 Texas 3-D Face Recognition Database

Our goal is to implement and evaluate face recognition algorithms which are intended to operate under real-world test conditions specified by NIST: where the only constraint is that subjects are asked to stand at a fixed distance from the cameras without wearing accessories such as glasses or hats and to face the camera. This is the assumption that is likely to be made in many applications such as access control to secure facilities or airport screening where the face recognition system operates in the presence of a human administrator and users are asked to have a certain degree of cooperation with the authorities. Since in such applications laser ranging would be inappropriate, NIST funded the construction of the Texas 3-D Face Recognition Database (T3FRD) (Gupta et al. 2010) which is the largest publicly available database of co-registered 2-D and 3-D face images acquired using a passive modality (i.e. optical stereo ranging).

Driven by our application scenario, we focus on the problem of recognition (including fiducial detection, feature extraction, statistical learning, and classification), and not pre-processing (scaling, alignment, rotation, etc.) of the face data. In our view, since pre-processing and recognition are largely separate problems, algorithms to accomplish these tasks should be tested separately. T3FRD is a large recently-released public database of co-registered 2-D and 3-D face

images that is finding significant use. T3FRD is available to researchers free of charge. It contains 1196 pairs of roughly aligned, high resolution, colored portrait and range images from 116 adult subjects. The images were captured at the former Advanced Digital Imaging Research (ADIR) LLC (Friendswood, TX) using a MU-2 stereo imaging system made by 3Q Technologies Ltd. (Atlanta, GA), under contract to NIST.

All the portrait and range pairs in the database are roughly aligned with respect to a fixed generic face in the canonical frontal pose using the iterative closest point (ICP) algorithm (Besl and McKay 1992). Since all of the 3-D facial images in T3FRD are aligned by an identical procedure, fair comparisons can be made between competing algorithms based on recognition capability only without biases introduced by pre-processing. The database include images of male and female subjects (68 % male and 32 % female) with ages ranging from 20 to 75 years old. About 80 % of the images in T3FRD are from subjects younger than 40 years of age. T3FRD contain images from different ethnicities with the following mix: 40 % of images are from Caucasian subjects, 5 % from Africans, 32 % from Asians, 22 % from East-Indians, and the rest belong to other ethnicities. The database contains 69 % neutral and 31 % expressive faces. Each range and portrait pair is accompanied by a file containing information about the subject's gender, ethnicity, facial expression, and manually annotated locations of 25 anthropometric facial fiducial points. Examples of range and colored portrait pairs are presented in Fig. 1. The left two columns are image pairs
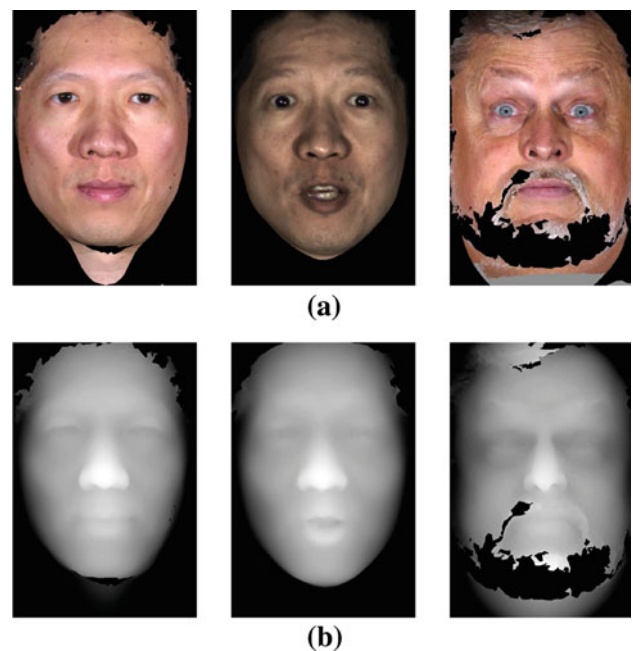

Fig. 1 Example of face images from the Texas 3-D Face Recognition Database (**a**) colored portrait images (**b**) The corresponding range images

from a single subject captured at two different sessions, one neutral and the other with an expression. The image pair in the rightmost column is an example of a subject with an expressive face and missing surface information on areas covered with facial hair.

T3FRD complements the older publicly available Face Recognition Grand Challenge (FRGC) 2005 database (Phillips et al. 2005) and is a good alternative for researchers who want to evaluate their innovative face recognition algorithms without dealing with extensive pre-processing such as head pose normalization and scaling as required by the FRGC dataset. Of course, for free-viewing scenarios of human faces, T3FRD is only appropriate for testing the recognition modules. Integrated pre-processing and recognition algorithms for free-viewing should be tested on FRGC. T3FRD allows isolation of face recognition performance without any bias introduced by choice of complicated pre-processing schemes. It is the largest (in terms of number of images and subjects) database that has been acquired using a stereo imaging system at a high resolution of 0.32 mm along the x, y, and z dimensions. By comparison, images in the FRGC database were acquired using a Minolta Vivid 900/910 laser scanner sampled at a lower average resolution of 0.98 mm along x and y dimensions and 0.5 mm along the z dimension (Chang et al. 2003).

Since stereo imaging captures both the shape and the portrait image of the face simultaneously, each range and portrait pair are perfectly co-registered in the T3FRD. By contrast, there was a significant time-lapse between the operation of the laser range finder and the optical camera in the FRGC data acquisition procedure, which caused the acquired 2-D and 3-D images in the FRGC be out of correspondence (Phillips et al. 2005). This time-lapse also caused inconsistencies in facial expression between the range and portrait images captured in a single subject session (Maurer et al. 2005). Since laser scanning is not instantaneous, some of the faces in the FRGC have been reported to be distorted due to head movements during acquisition (Maurer et al. 2005). Finally, 3-D face acquisition using laser range finders can cause emotional or physical discomfort in those being scanned, and in our view, is a modality that is highly unlikely to be deployed often in practice at least in our application scenario. Much of the pre-processing required to utilize the FRGC database is unlikely to be required using a passive sensing system, such as stereo ranging systems.

A few pre-processing steps are performed on all of the T3FRD range images: First, extraneous background regions that are not connected to the face are removed by detecting the face as the biggest connected blob having non-zero range value, and eliminating all remaining smaller blobs. Impulse noise present in the range images are removed by median filtering with a 3×3 square filter. Holes and areas with missing data are filled by bi-cubic interpolation. All images in the database are of size 751×501. The z value in the range images is represented using 8 bit format with closest point to the camera having the highest value of 255. In our experiments, we reduced the size of all images by a factor of 3 in each direction to reduce computational cost, so the resulting images used were of size 251×167 pixels.

4.2 Automatic Facial Landmark Detection

The automatic detection of fiducials plays an important role in many face related applications. There are very few techniques proposed in the literature that use 3-D or combination of 2-D and 3-D facial clues for fiducial detection. In this article, the algorithm that we proposed in (Jahanbin et al. 2008) is used to detect three fiducials using Gabor responses extracted from range images. This fiducials are: the nose tip (NT), the left eye inner corner (LEIC), and the right eye inner corner (REIC). With highly competitive accuracy, this landmark detection technique has been adopted for other approaches to face recognition and related applications (Gupta et al. 2010; Moorthy et al. 2010).

The local appearance around a point, $\mathbf{x}$, in a range image is encoded using a set of 40 Gabor coefficients, a Gabor "jet", derived by convolving the input image with a family of Gabor kernels covering 5 spatial frequencies and 8 orientations. In other words, a "jet" $\mathbf{J}$ is a set $\{J_j, \ j = u + 8v\}$ of 40 complex Gabor coefficients obtained from a single image point. Complex Gabor coefficients are represented as $J_j = a_j \exp(i\phi_j)$ where $a_j(\mathbf{x})$ is the slowly varying magnitude and $\phi_j(\mathbf{x})$ is the phase of the jth Gabor coefficient at $\mathbf{x}$.

A phase sensitive similarity metric is used to measure similarity between any two Gabor jets:

$$S(\mathbf{J}, \mathbf{J}') = \frac{\sum_{i=1}^{40} a_i \acute{a}_i \cos(\phi_i - \acute{\phi}_i)}{\sqrt{\sum_{i=1}^{40} a_i^2 \sum_{i=1}^{40} \acute{a}_i^2}} \tag{1}$$

This similarity measure returns real values in the range $[-1, +1]$, where a value close to $+1$ means a high similarity between the input jets.

An appearance modeling template, called a "Gabor bunch", is created for each detectable fiducial by manually marking that fiducial on a small training set containing 50 range images from the available 1196 range images in T3FRD. Finally, Gabor jets calculated from 50 training images at the manually marked landmarks from a specific feature point (e.g. nose tip) are stacked together to create a bunch representation of that fiducial. For example, the nose tip's bunch describes the nose tip in the range images.
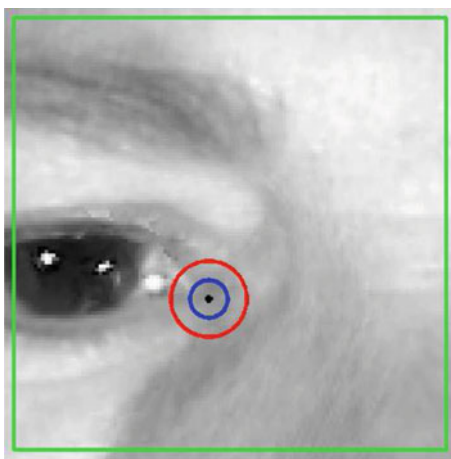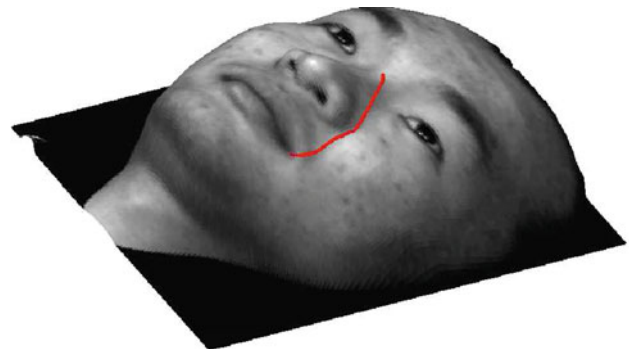
In order to automatically locate a fiducial point on a range image which has never been seen before, the range data enclosed by the search area of that feature point are first convolved with the set of 40 Gabor wavelets. As a result,

Table 1 Statistics of the Euclidean distance between the automatically detected feature points and the manually labeled ground-truth

Fiducial	Mean (mm)	Std. (mm)
LEIC	1.65	1.7
REIC	1.63	1.5
NT	1.40	0.9

each pixel of the search area is represented by a "range jet". Next, The jets are compared to their corresponding bunch and a similarity map is created demonstrating the similarity between each pixel in the search area and the bunch. Fiducial point detection is done by picking the pixel having the highest similarity value.

The accuracy of the proposed fiducial detection algorithms was evaluated using the remaining 1146 range images from T3FRD by measuring the positional error between detected landmarks and manually annotated ground-truth in millimeters (mm). Table 1 provides statistics on the positional error occurred in the detection of LEIC, REIC, and NT. It is interesting to note that each of the three fiducials of interest in our iso-geodesic based face recognition system is detected with very high accuracies (average positional error less than 1.65 mm). The accuracy of the utilized fiducial point detection algorithm can be visualized by Fig. 2, which shows the search box for the left inner corner of the eye (LEIC) on an arbitrary portrait image where the correct location of LEIC is marked with a black dot. The radius of the blue circle (inner circle) in is equal to 1.65 mm which is the mean positional error of detection on LEIC using range information (Table 1). The red circle (outer circle) has a radius equal to mean 1.65 mm plus one standard deviation 1.7 mm.

Fig. 2 Correct location of LEIC is shown with a *black dot* in the search area marked with *green square*. The *blue circle* (*inner circle*) shows the mean positional error and the *red circle* (*outer circle*) marks the mean plus one standard deviation of the positional error (Color figure online)

Fig. 3 Shortest path between the nasion point and right mouth corner shown on an arbitrary face

4.3 Iso-Geodesic Contours

In order to extract iso-geodesic contours around LEIC, REIC, and NT, the first step is to calculate the geodesic distance between the landmark and any available point on the facial surface. The geodesic distance between two points on a surface is the length of the shortest path connecting those two points on that surface. Figure 3 shows the shortest path between the nasion point and a mouth corner on an arbitrary face in the database. We define an iso-geodesic contour to be a loci of all points on the surface having the same geodesic distance from a given origin. Given a facial surface (a domain) Ω and a fiducial point (source point) X_0, it is desirable to find the shortest distance between each point $X \in \Omega$ from X_0, $D(X)$. The problem is formulated by the *Eikonal* equation:

$$\|\nabla_\Omega D(X)\| = P, \quad D(X_0) = 0 \qquad (2)$$

This equation describes the propagation and evolution of a wavefront through a medium and the parameter P is a constant showing the velocity of the wave propagation. An efficient algorithm to solve the *Eikonal* equation is the "Fast Marching" method proposed by Kimmel and Sethian (1998). The Fast Marching Method simulates an imaginary scenario in which a bad guy sets a fire at source point X_0 at time $t = 0$ to a uniformly distributed forest Ω. The fire front advances outwards from the source point, while firemen register the time $T(X)$ at which fire arrives at location X. Once a point is touched by fire, the trees burn out and the fire never again visits the location where it had already passed. The distance $D(X)$ is proportional to the reaching time $D(x) = P \cdot T(X)$. The Fast Marching Method finds the geodesic distance from a source point to n grid points defined on the surface in $O(n)$ operations.

We used Peyré and Cohen's (2006) Matlab toolbox which is capable of performing Fast Marching on surfaces defined on either rectangular or triangular domains to calculate geodesic distance maps with respect to NT, LEIC, and REIC. Figure 4 shows an example range image along with geodesic
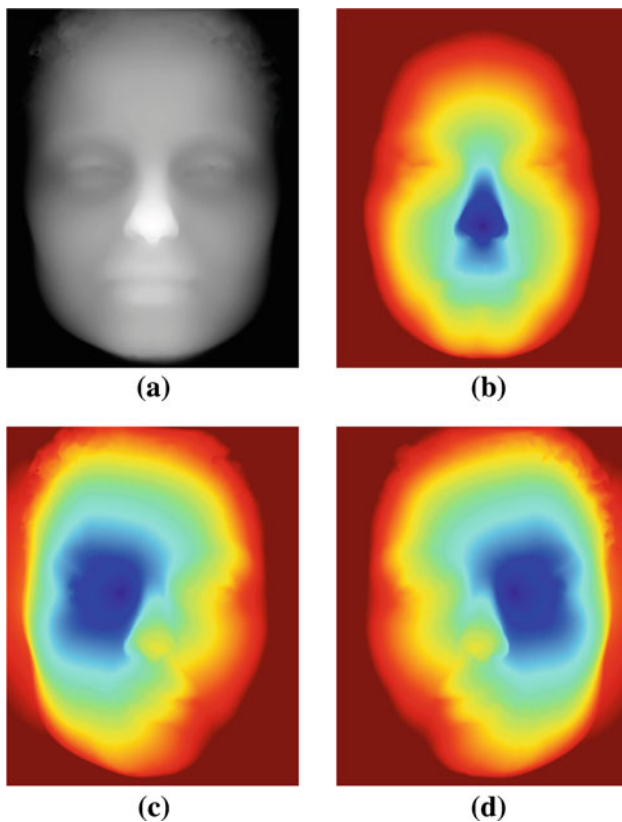
Fig. 4 An example range image from the database and corresponding geodesic distance maps. *Dark blue* (*dark in black* and *white printout*) reflects shorter distance and *red* (*light in black and white printout*) means farther distance (**a**) range image (**b**) Geodesic distance map from NT (**c**) Geodesic distance map from LEIC (**d**) Geodesic distance map from REIC (Color figure online)

distance maps from LEIC, REIC, and NT. The dark blue regions (dark in black and white printout) represent smaller distances and red (light in black and white printout) means farther distances.

After obtaining a geodesic distance map, its values are normalized with a fixed reference distance measured between two landmarks on that subject's face. This step is crucial to reduce the unwanted effects that subjects' head size variation, due to the distance variation between subjects and scanner, has on the shape and size of the extracted contours. The geodesic values in a NT geodesic distance map are normalized by the average geodesic distances between the nose tip and the outer eye corners of that subject. Values in LEIC and REIC geodesic distance maps are normalized by the average geodesic width of the subject's eyes. Finally, the iso-geodesic contours are extracted from normalized distance maps by finding the the boundaries of objects created by thresholding normalized distance maps using thresholds $d = 1/3, d = 2/3$, and $d = 1$. Figure 5 shows all iso-geodesic contours extracted from an example range image from T3FRD overlaid on the input range image.
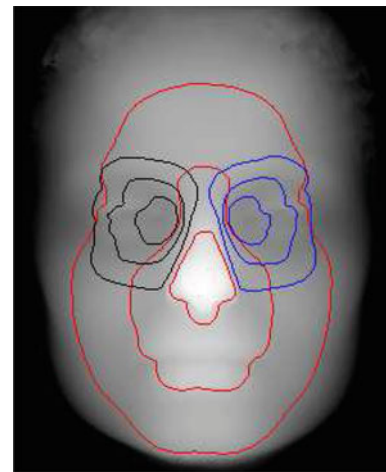

Fig. 5 Example of a range image with iso-geodesic contours extracted from around NT, LEIC, and REIC

The extracted 3-D iso-geodesic contours are next smoothed and fitted by cubic splines and then parameterized by arc length ℓ:

$$C(\ell) = \{x(\ell), y(\ell), z(\ell)\}^T , \quad 0 \leq \ell \leq 1. \tag{3}$$

Having access to cubic spline fits makes it easier to sample iso-geodesic contours at any given number of points with any desired arc length interval distribution.

5 Feature Extraction

In our earlier iso-geodesic face recognition algorithm (Jahanbin et al. 2008) as well as many other contour-based face recognition algorithms in the literature (Samir et al. 2006; Mpiperis et al. 2007; Sun and Abidi 2001), features are extracted from the projection of contours onto a reference plane (e.g. tangent plane at the center) because it is easier to process planar contours. This transformation from 3-D to planar contours results in the loss of important contour characteristics and vulnerability against pose variations owing to uncertainty in finding the reference projection plane. Here we use simple, innovative and effective features that are directly extracted from 3-D contours, thereby preserving the important pose invariance quality of iso-geodesic contours.

5.1 Radial Euclidean Distances

One set of pose-invariant features that we use are the Euclidean distances measured in a three-dimensional coordinate system from the origin of the iso-geodesic contours. First, each contour is divided into 60 intervals with equal arc-lengths. Next, the lengths of 60 vectors connecting the origin of the contour, $O(x_o, y_o, z_o)$, to equal arc-length sample points, $P_i(x_i, y_i, z_i)$, are organized in a feature vector,
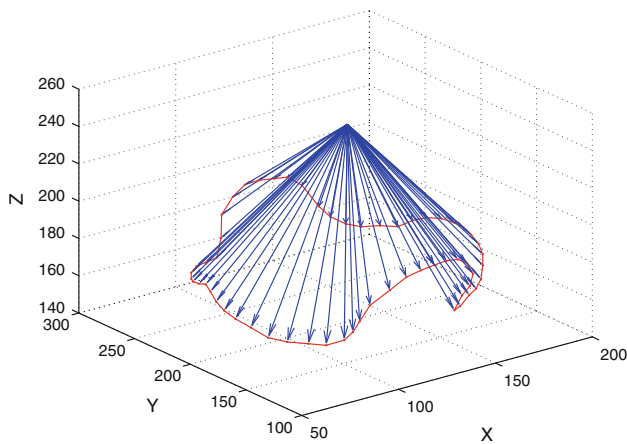
Fig. 6 Radial Euclidean distances between the nose tip and equal arc-length sample points on an iso-geodesic facial contour

Fig. 7 Example facial contour around the nose tip and tangent vectors along the path

$\mathbf{d} = \{d_i\}$, $i = 1, 2, \ldots, 60$, encoding the shape of the iso-geodesic contour:

$$d_i = \sqrt{(x_i - x_o)^2 + (y_i - y_o)^2 + (z_i - z_o)^2} \qquad (4)$$

Figure 6 shows an example facial contour extracted from the region around the nose tip and the corresponding 60 vectors originating from the center.

5.2 Curvatures Along the Contour

Another set of valuable contour attributes is obtained by calculating the curvatures along the contour path. Curvatures are extracted using the Frenet-Serret formulas in three-dimensional Euclidean space by first calculating unit length tangent vectors, $\mathbf{T}$, pointing in the counter-clockwise traversal at each equal arc-length sample point. According to the Frenet-Serret formulas, the curvature is

$$\kappa = \left\| \frac{d\mathbf{T}}{d\ell} \right\| \qquad (5)$$

where ℓ is the arc-length parameter. Figure 7 shows an example facial contour in the region around the nose tip with tangent vectors indicated along the contour by arrows.

5.3 Distances from a Procrustean Circle

A considerable amount of work in the literature has been devoted to defining planar shape descriptors by comparing them against primitive shapes, such as circle, ellipses, and triangles (Peura and Iivarinen 1997; Rosin 2003). Here we extend this general concept to define innovative shape descriptors of 3-D contours as explained in Sects. 5.3–5.5. The comparison of iso-geodesic contours against a circle in three-dimensional Euclidean space is performed using Procrustes analysis. First, a unit circle is sampled using the
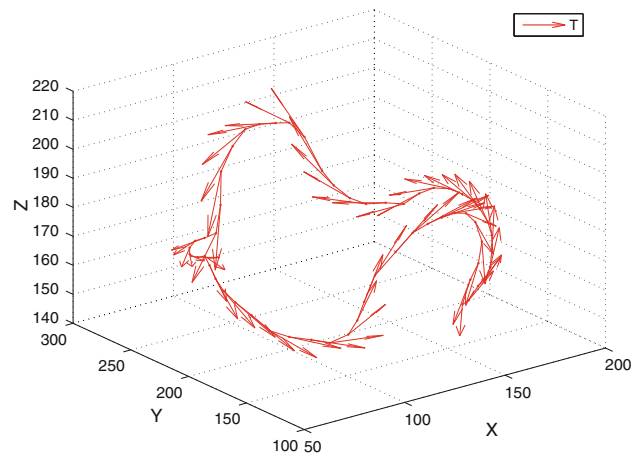
same number of points present on the input contour (i.e. 60 equal arc-length sample points). Then, the unit circle undergoes a series of shape-preserving Euclidean transformations (translation, reflection, orthogonal rotation, and scaling) to best conform to the input contour by minimizing the sum of squared distances between corresponding points. Finally, Euclidean distances measured between each point on the iso-geodesic contour, $P_i(x_{pi}, y_{pi}, z_{pi})$, $i = 1, 2, \ldots, 60$, and the transformed circle points, $C_i(x_{ci}, y_{ci}, z_{ci})$, $i = 1, 2, \ldots, 60$, are collected in a 60 dimensional feature vector $\mathbf{d} = \{d_i\}$, $i = 1, 2, \ldots, 60$ where

$$d_i = \sqrt{(x_{pi} - x_{ci})^2 + (y_{pi} - y_{ci})^2 + (z_{pi} - z_{ci})^2} \qquad (6)$$

Figure 8 shows an example facial contour in the region around the nose tip with arrows indicating the distance between corresponding points on the contour and the Procrustean fitted circle.
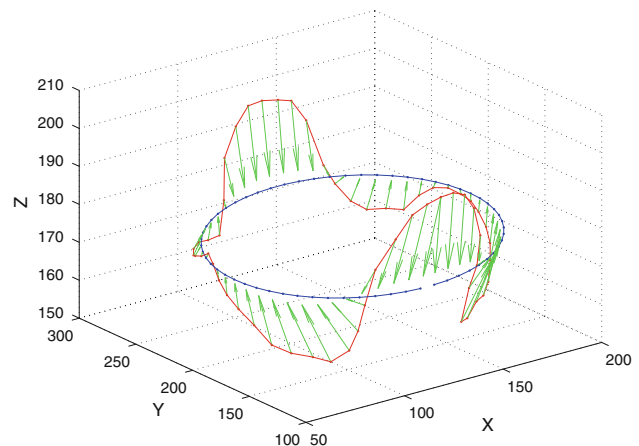

Fig. 8 Example facial contour around the nose tip with *arrows* showing the distance between corresponding points on the contour and the Procrustean fitted circle

5.4 Distances from Procrustean Ellipses

Another class of geometrical shapes commonly used in shape analysis comparisons is the ellipsoid family (Peura and Iivarinen 1997; Rosin 2003), which possess a higher degree of freedom as compared to circles by allowing elongation. Comparison and approximation of a planar contour with a set of ellipses is the fundamental idea behind Elliptical Fourier Transforms (EFT) (Kuhl and Giardina 1982). Here, features are obtained by fitting a horizontal and a vertical ellipse with eccentricity equal to $\epsilon = \frac{\sqrt{3}}{2}$ to the input contour using Procrustes analysis. First, the ellipse (vertical or horizontal) is sampled with the same number of points as the input contour (i.e. 60 equal arc-length sample points). The ellipse sampled at an ordered set of points is transformed by Procrustes analysis to best conform to the input contour by minimizing the sum of squared distances between corresponding points. Finally, Euclidean distances measured between each point on the iso-geodesic contour, $P_i(x_{pi}, y_{pi}, z_{pi}), i = 1, 2, \ldots, 60$, and the transformed ellipse sample points, $E_i(x_{ei}, y_{ei}, z_{ei}), i = 1, 2, \ldots, 60$, are collected in a 60-dimensional feature vector $\mathbf{d} = \{d_i\}, i = 1, 2, \ldots, 60$ where

$$d_i = \sqrt{(x_{pi} - x_{ei})^2 + (y_{pi} - y_{ei})^2 + (z_{pi} - z_{ei})^2} \tag{7}$$

Figure 9 shows an example facial contour around the nose tip with arrows showing the distance between corresponding points on the contour and a Procrustean fitted ellipse.

5.5 Procrustes Scales and Errors

From each Procrustes analysis in Sects. 5.3 and 5.4, two additional features can be obtained, the fitting scale and the residual error. Combining circular and elliptical Procrustes analy-
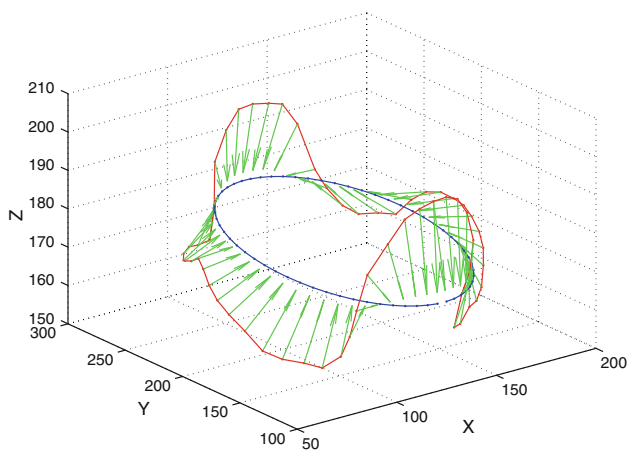
ses, a six-dimensional feature vector comprised of circular scale, circular residual error, horizontal elliptical scale, horizontal elliptical residual error, vertical elliptical scale, and vertical elliptical residual error is collected from each contour. Intuitively, the elliptical scales and residual errors are indications of elongation in the vertical and horizontal directions. Circular scales and residual errors reflect the compactness and roundness of the contours.

6 Performance Evaluation Methodology and Data

We combine iso-geodesic contour features in a hierarchical scheme to create a unified face recognition system (Sect. 7). First, each feature category is evaluated around the fiducial points and the results are reported independently. Next, features extracted from around the same landmark are fused to create three parallel face recognition systems (one per fiducial). Finally, these three face recognizers are merged to create a unified face recognition system. The details of this hierarchical scheme and the evaluation results at each stage are discussed in Sect. 7.

In this section, the data and the methodology used to evaluate the performance of the proposed algorithms are described. In Sect. 6.1, the breakdown of T3FRD into training and testing sets is explained. Section 6.2 explains how the performance of a face recognition system is measured in identity verification and identification scenarios according to established face recognition protocols (Moon and Phillips 1998). The classification task is performed by a 1NN classifier using Euclidean distance metric in LDA subspace as explained in Sect. 6.3.

6.1 Face Recognition Data

In order to evaluate the verification and identification performance of the proposed features, the 1196 range images from 116 subjects present in T3FRD were partitioned into disjoint training and testing sets. The training set contained 270 range images from 18 subjects (15 per subject). The training set was used by the stepwise-LDA (Sharma 1995) to select the most discriminative subset of features from raw concatenated features. Also, the training set was used to design 1NN classifiers using Euclidean distance metric in LDA subspace. The test set was further divided into a gallery set and a probe set. The gallery set contained 103 range images from 103 individuals (1 image per subject) who have at least 2 range images in the test set. The probe set has 810 range images from the 103 enrolled subjects in the gallery set, where the number of range images per subject varies, with a minimum of 1 image for some subjects to maximum of 77. There are 13 subjects in T3FRD with only 1 range image per subject, which are included as imposters in the probe set.

Fig. 9 Example facial contour around the nose tip with *arrows* showing the distance between corresponding points on the contour and a Procrustean fitted ellipse

6.2 Verification and Identification Tasks

In verification scenarios (e.g. access control systems), a face recognition system compares the retrieved features of the claimed identity (from the gallery set) with the currently captured features of the user and declares a match if features are more similar than a given threshold. The performances of face recognition algorithms in the verification experiment are usually described by the receiver operation curve (ROC). The ROC curve plots the false acceptance rate (FAR) against the false rejection rate (FRR) for various operating thresholds. Two quantitative measures of verification performance, the equal error rate (*EER*) and area under the curve (*AUC*), are accepted measures of overall face recognition performance that we have adopted (Egan 1975). Both the *AUC* and *EER* performance metrics of a face recognition system approach zero as the system approaches an ideal.

In the Identification scenario, the features of the subject are compared against the enrolled models in the gallery set and the results are ranked based on the similarity scores. The identification performance of the proposed algorithms are expressed by the cumulative match characteristic (CMC) curves and the rank 1 recognition rates (*RR*1) (Grother et al. 2003).

6.3 Euclidean Distance Decision Rule in LDA Subspace

We use Fisher's LDA to project features selected by stepwise-LDA to lower-dimensional feature spaces that maximize the between-class scatter, S_b, while minimizing the within-class scatter, S_w. The projection directions are learned only from the training portion of the dataset. In the evaluation phase, features from faces in the testing set are first projected onto the LDA subspace using the projection directions learned in the training session. The authentication and identification tasks are performed based on the measured Euclidean distances in the lower dimensional LDA subspace between currently captured features and features retrieved from people enrolled in gallery.

7 Results

In order to construct a unified 3-D face recognition system, the multiple feature types (Sect. 5) collected around 3 landmarks at 3 different geodesic radii are hierarchically fused as illustrated by Fig. 10. In this hierarchy, the first stage of fusion takes place by merging one type of feature from contours of all radii around each fiducial origin (e.g. curvatures from NT contours 1–3 as shown in Fig. 10). A performance evaluation of the first fusion stage, called "Contour Scale Fusion", are presented in Sect. 7.1. In the next stage of the hierarchy, "Fiducial Scale Fusion", all of the fused features collected around each fiducial point are merged into a single concise feature vector (one per fiducial) specialized to describing the immediate vicinity of that fiducial (Sect. 7.2). At the highest stage of the hierarchy, "Global Scale Fusion", three parallel face recognition systems are fused by feature-level and match score-level techniques into two alternative unified face recognition systems.
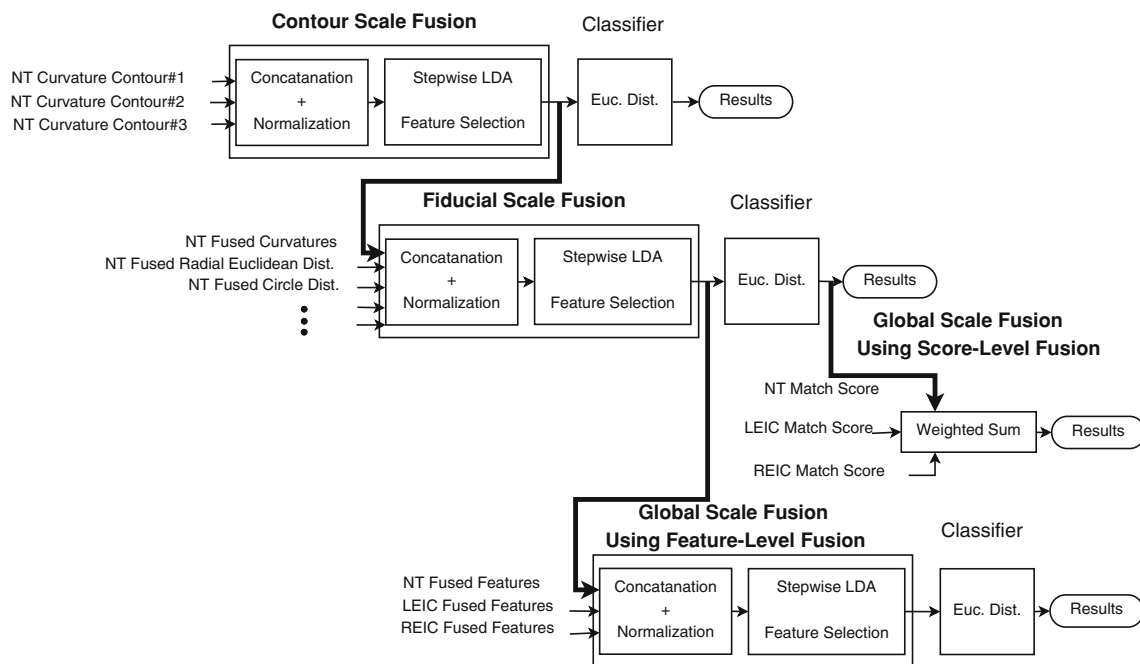

Fig. 10 The proposed hierarchical feature fusion scheme

7.1 Contour Scale Fusion

Features from the same category calculated around each fiducial are merged using a feature-level fusion technique (Ross et al. 2006). The feature-level fusion technique used in this stage, as well as in higher stages of the proposed hierarchy, are illustrated in Fig. 10. First, all collected features are concatenated and normalized to a common range using *min–max* normalization. The parameters of the normalization are learned from the training set. The normalization step is important to prevent features having greater numeric ranges from dominating those having smaller ranges. Finally, stepwise-LDA (Sharma 1995) is applied to reduce the dimensionality of the raw feature vectors by picking the most discriminative subset of features. The stepwise-LDA was accomplished with the STEPDISC procedure in SAS software (SAS Institute, Cary, NC). Stepwise-LDA feature selection starts with an empty set of features. At each step, the best feature that is not currently in the set is added to the set if its significance level is higher than the "entry significance level". At each step, features from the selected set that are no longer among the best are removed if their significance level is below the "exit significance level". Feature significance levels at each step are calculated based on Wilks' lambda statistic (Sharma 1995). The procedure terminates when no more features can be added or removed based on the specified significance level for entry and removal of features. In our implementation, both significance levels are set to 0.05. The subset of features selected by stepwise-LDA have reasonably low dimensionality and can be used by a 1NN classifier using Euclidean distance metric in LDA subspace as explained in Sect. 6.3, without facing the "small sample size" prob-

lem (Duda et al. 2001). The dimensionality of the features selected by stepwise-LDA is not known a priori and it differs from one category of features (e.g. Radial Distance from LEIC) to another (e.g. NT Curvatures). We have observed a range of about 30–50 features being selected from different categories.

The verification and identification performance of contour features collected around automatically detected LEIC are displayed by CMC and ROC curves in Fig. 11. Table 2 presents the EER, AUC, and RR1 values for each feature category. Among the features collected around the LEIC, the "Horizontal Ellipse Procrustes Distances" have the best verification performance closely followed by the "Vertical Ellipse Procrustes Distances" and the "Circle Procrustes Distances". After these three leading features, a second tier of features is identifiable which consists of the "Procrustes Scales & Errors" and the "Radial Distances from LEIC". Finally, the poorest performing features around the LEIC are the "Curvatures along the contour". The same trend is observed for the identification performance of features extracted around the LEIC, where the "Horizontal Ellipse Procrustes Distances" has the best performance ($RR1 = 90.94\%$) followed by the "Vertical Ellipse Procrustes Distances" and the "Circle Procrustes Distances" ($RR1 = 89.13\%$ and $RR1 = 87.92\%$, respectively). The only exception is that the lowest performing feature from the LEIC in identification task is the "Procrustes Scales & Errors" with $RR1 = 66.93\%$.

Figure 12 and Table 3 present the identification and verification performance of features collected around the automatically detected REIC. Similar to LEIC, three tiers of features are identifiable based on their verification performance
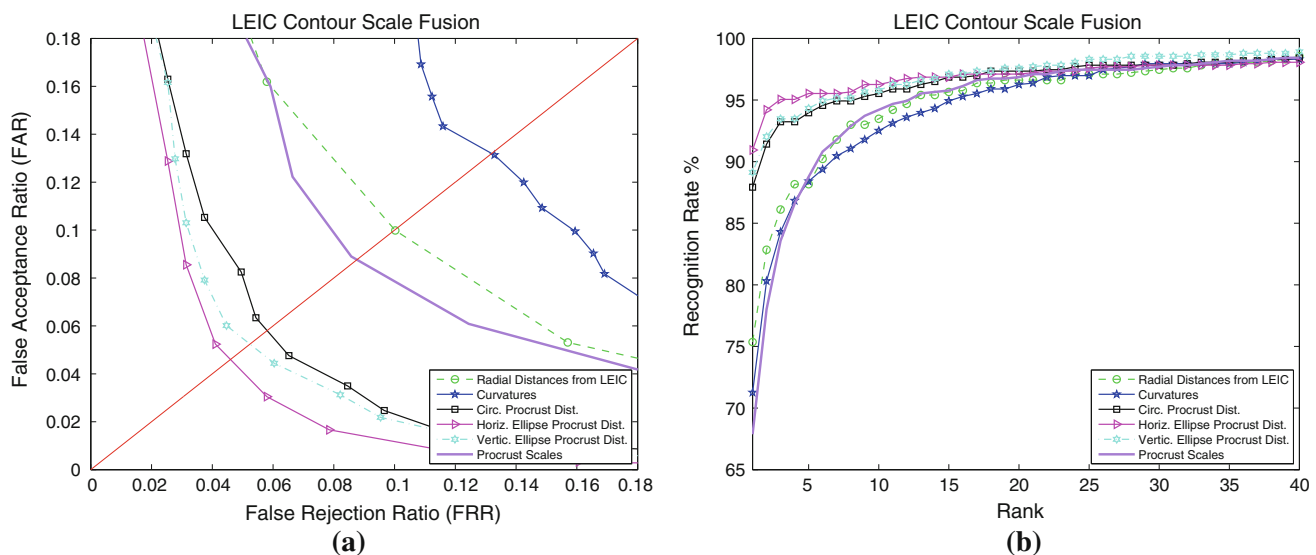

Fig. 11 Performance evaluation of Contour Scale Fused features collected around automatically detected LEIC: (**a**) ROC curves showing the verification accuracies (**b**) CMC curves showing the identification performance

Table 2 The observed EER, AUC, and RR1 values for automatically detected LEIC features

Algorithm	EER (%)	AUC	RR1 (%)
Curvatures	13.20	0.0645	71.26
Radial Distance from LEIC	10.01	0.0367	75.36
Procrustes Scales and Errors	8.76	0.0369	66.93
Circular Procrustes Dist.	5.80	0.0192	87.92
Verti. Elliptical Procrustes Dist.	5.24	0.0148	89.13
Horiz. Elliptical Procrustes Dist.	4.60	0.0132	90.94

Table 3 The observed EER, AUC, and RR1 values for automatically detected REIC features

Algorithm	EER (%)	AUC	RR1 (%)
Curvatures	14.23	0.0909	64.97
Radial Distance from REIC	9.03	0.0348	78.62
Procrustes Scales and Errors	8.70	0.0363	67.87
Circular Procrustes Dist.	6.55	0.0223	84.54
Verti. Elliptical Procrustes Dist.	6.14	0.0213	87.07
Horiz. Elliptical Procrustes Dist.	5.92	0.0178	88.04

(Fig. 12a; Table 3). In the highest performing tier, the "Horizontal Ellipse Procrustes Distances" have the best verification performance closely followed by the "Vertical Ellipse Procrustes Distances" and the "Circle Procrustes Distances". The "Procrustes Scales & Errors" and the "Radial Distances from REIC" are in the second tier. Finally, the "Curvatures along the contour" from REIC supplies the worst performance. The same general trend is observed for the identification performance of features extracted around REIC, where the "Horizontal Ellipse Procrustes Distances" has the best performance ($RR1 = 88.04\%$) followed by the "Vertical Ellipse Procrustes Distances" and the "Circle Procrustes Distances" ($RR1 = 87.07\%$ and $RR1 = 84.54\%$, respectively). The lowest performing feature from REIC in identification task is again the "Curvatures along the contour" ($RR1 = 64.97\%$).

Figure 13 and Table 4 display and summarize the performance evaluation of features collected around automatically detected NT. For comparison purposes, two baseline face classifiers, the Eigensurfaces (Russ et al. 2006; Hesher

2003) and the Fishersurfaces (Gokberk et al. 2005; Heseltine et al. 2004), were implemented by applying PCA and LDA to the range images after performing the alignment proposed by Russ et al. (2006). The performance of these baseline algorithms are presented in Fig. 14 and Table 5. In the verification task, the "Radial Distances from NT" and the "Horizontal Ellipse Procrustes Distances" present notable performance among the features computed around automatically detected NT. The "Vertical Ellipse Procrustes Distances", the "Circle Procrustes Distances', and the "Procrustes Scales & Errors" closely follow, while again the "Curvatures along the contour" has the poorest performance. In the identification evaluation of NT features, the "Radial Distances from NT" and the "Horizontal Ellipse Procrustes Distances" are the best performing NT features ($RR1 = 97.82\%$ and $RR1 = 96.98\%$, respectively).

It is interesting to observe that some of the features collected around NT, such as the "Radial Distances from NT", the "Horizontal Ellipse Procrustes Distances", and the "Vertical Ellipse Procrustes Distances" perform better than the
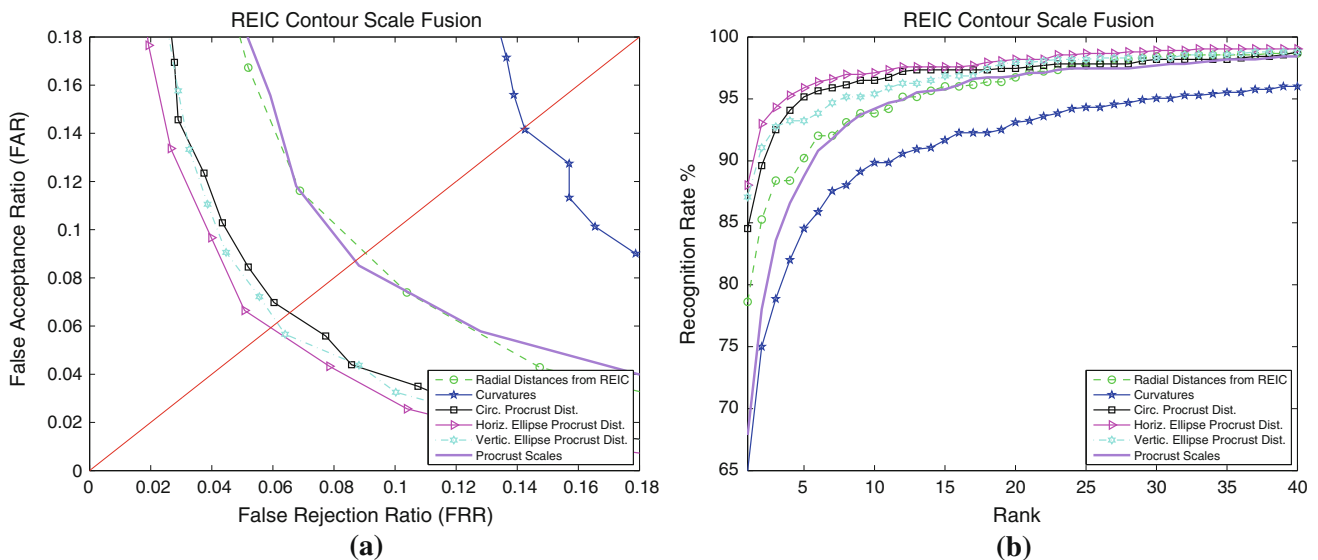

Fig. 12 Performance evaluation of Contour Scale Fused features collected around automatically detected REIC: (**a**) ROC curves showing the verification accuracies (**b**) CMC curves showing the identification performance
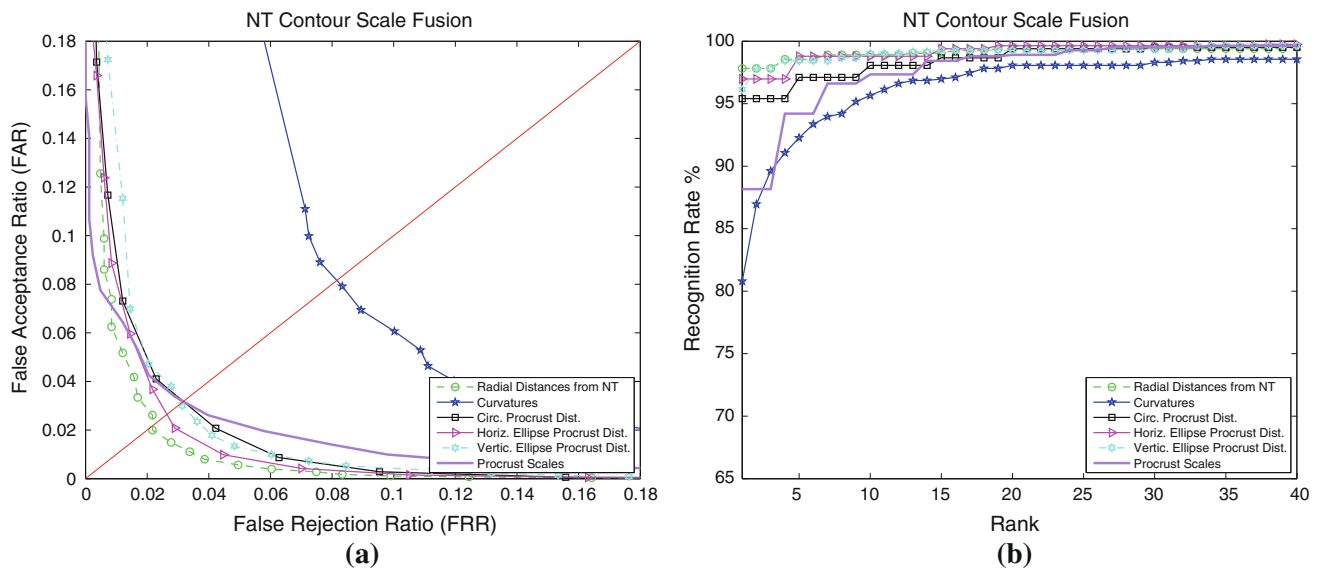
Fig. 13 Performance evaluation of Contour Scale Fused features collected around automatically detected NT: (**a**) ROC curves showing the verification accuracies (**b**) CMC curves showing the identification performance

Table 4 The observed EER, AUC, and RR1 values for automatically detected NT features

Algorithm	EER (%)	AUC	RR1 (%)
Curvatures	8.16	0.0345	80.79
Procrustes Scales and Errors	3.18	0.0042	88.16
Radial Distance from NT	2.17	0.0033	97.82
Circular Procrustes Dist.	3.18	0.0037	95.41
Verti. Elliptical Procrustes Dist.	3.10	0.0047	96.13
Horiz. Elliptical Procrustes Dist.	2.64	0.0029	96.98

benchmark Eigensurfaces and Fishersurfaces in both identification and verification evaluations, because iso-geodesic contours are more robust against the pose variations and facial expression changes present in T3FRD. This observation becomes more striking when it is considered that the total number of points on NT iso-geodesic contours are only a very small fraction of data used by benchmark algorithms. Another important observation is that any feature from around NT outperforms its LEIC and REIC counterpart in terms of the *EER*, *AUC*, and *RR*1 performance measures. This phenomena can be explained by the fact that iso-geodesic contours cover a larger area of the face while the LEIC and REIC contours are limited to the small eye socket area (Fig. 5).

7.2 Fiducial Scale Fusion

In the "Fiducial scale Fusion" stage of the hierarchy, all of the features combined in the previous stage ("Contour Scale Fusion") are merged into three concise feature sets (one per

automatically detected fiducial) specialized to describe the immediate vicinity of that fiducial. The fusion technique used in this stage is the same feature-level fusion scheme used in the "Contour Scale Fusion". First, all the fused features from a fiducial are concatenated and normalized to a common range using *min–max* normalization. Stepwise-LDA is applied to perform the final step of the fusion by keeping the most discriminative subset of features while discarding the rest.

The identification and verification performance of the face recognizers at this stage are presented in Fig. 14 and Table 5. The "NT" fused features managed to achieve $EER = 1.40$ and $AUC = 0.00230$ in the identification task and $RR1 = 98.18\%$. By comparing this result with the results in Fig. 13 and Table 4, it is clear that the NT face recognizer performs better than any individual NT feature contributing to the system. Also comparing the NT face recognizer's performance with the benchmark Fishersurfaces and Eigensurfaces (Fig. 14; Table 5), it is clear that the NT face recognizer performs far better than the benchmarks. Similarly the LEIC and REIC attain performance measures ($EER = 3.23\%$, $AUC = 0.0093$, $RR1 = 91.06\%$) and ($EER = 3.97\%$, $AUC = 0.0120$, $RR1 = 90.82\%$) that are greatly improved compared to their individual constituent features. The performance of the LEIC and REIC fused face recognizers are comparable to the Fishersurfaces algorithm and much better than Eigensurfaces.

7.3 Global Scale Fusion

Finally, at the highest stage of the proposed hierarchy, the NT, LEIC, and REIC classifiers are combined to create a
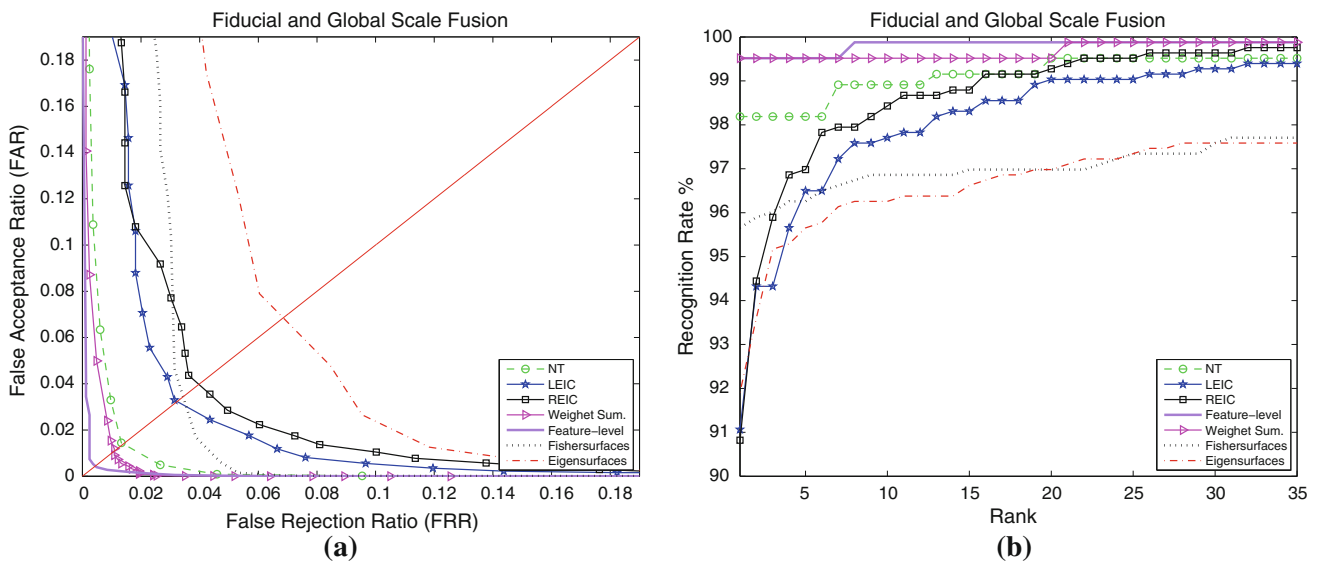
Fig. 14 Performance evaluation of the "Fiducial Scale Fusion", the "Global Scale Fusion", and the benchmarks with automatically detected landmarks: (**a**) ROC curves showing the verification accuracies (**b**) CMC curves showing the identification performance

Table 5 The observed EER, AUC, and RR1 values for the "Fiducial Scale Fusion", the "Global Scale Fusion", and the benchmarks with automatically detected landmarks

Algorithm	EER (%)	AUC	RR1 (%)
LEIC	3.23	0.0093	91.06
REIC	3.97	0.0120	90.82
NT	1.40	0.0023	98.18
Eigensurfaces	6.85	0.0293	91.90
Fishersurfaces	3.44	0.0143	95.65
Match score-level	1.09	0.0010	99.51
Feature-level	0.44	0.0003	99.51

single face recognition system. Two commonly used classifier fusion techniques, the feature-level and the match score-level, are implemented independently and their performances are compared. The feature-level fusion scheme used in this stage is the same as the previous stages. Features selected by NT, LEIC, and REIC face recognizers are concatenated and normalized. Stepwise-LDA is utilized to perform the final feature-level fusion by selecting the the most discriminating subset of features while discarding the rest.

Many different match score-level fusion techniques are proposed in the literature to integrate information available at the output of multiple classifiers into a more accurate unified system (Ross et al. 2006). In this study, we use the weighted sum approach to combine the following classifiers: (1) NT, (2) LEIC, (3) REIC. The match scores that are fused in this study are the Euclidean distances, $d_i, i = 1, 2, 3$, measured by each classifier. However, a combination of distances (match scores) is only meaningful when the distances

are in the same range. We have used *min–max* normalization to transform distances obtained from each classifier to a common range. The weighted sum fusion of distances, D_f, is then calculated:

$$D_f = \sum_{j=1}^{3} w_j * d_j^n \qquad (8)$$

where d_j^n and w_j are the normalized distance and weight of the jth classifier, respectively, with the condition $\sum_{j=1}^{3} w_j = 1$. Each classifier's weight is a function of its performance estimated using the training data:

$$w_j = \frac{1 - (FAR_j + FRR_j)}{3 - \sum_{i=1}^{3}(FAR_i + FRR_i)} \qquad (9)$$

where FAR_i and FRR_i are the false acceptance and false rejection rates of the ith classifier. We have used constant EER_i instead of FAR_i and FRR_i which are threshold dependent. The weights calculated for "NT", "LEIC", and "REIC" are $w_1 = 0.3437$, $w_2 = 0.3307$, and $w_3 = 0.3255$, respectively, indicating the importance and contribution of each classifier in this fusion.

Figure 14 and Table 5 summarize the performance of the alternative fusion schemes at the final stage, and compare them with each individual feature set or classifier contributing to the fusion. The match score-level fusion improves the verification performance measures to $EER = 1.09\%$, $AUC = 0.0010$ and increases the identification performance to $RR1 = 99.51\%$ which is better than the best performing individual classifier in the union (NT with $EER = 1.40\%$, $AUC = 0.0023$, $RR1 = 98.18\%$). However, feature-level

fusion leads to remarkably better performance: $EER = 0.44\%$, $AUC = 0.0003$, $RR1 = 99.51\%$.

The better performance of feature-level fusion is explainable by the fact that feature-level fusion takes place before classification, when richer information about the input patterns is available as compared to match score-level fusion which is a post-classification fusion based on abstract information about the inputs. In general, fusion techniques that integrate information at earlier stages of processing are believed to be more effective than systems which perform integration at a later stage (Ross et al. 2006). The final feature-level fused classifier achieve excellent performance with $EER = 0.44\%$ and $AUC = 0.0003$ and $RR1 = 99.51\%$.

7.4 Comparison to Other Works

Table 6 and Fig. 15 compare the results of the proposed iso-geodesic Procrustean contour based 3-D face recognition algorithm with several state-of-the-art algorithms that

Table 6 The observed EER, AUC, and RR1 values for algorithms evaluated on the Texas 3-D Face Recognition Database

Algorithm	EER (%)	AUC	RR1 (%)
Feature-level fused iso-geodesuc	0.44	0.0003	99.51
"Anthroface 3D" (Gupta et al. 2010)	1.65	0.0014	97.3
Warped Examples (Zou et al. 2007)	2.5	NA	NA
McKeon and Russ (2010)	0.42	0.0007	99.86
Mahoor and Abdel-Mottaleb (2009)	1.39	0.0023	98.19
Queirolo et al. (2010)	0.46	0.0003	NA

have been evaluated on T3FRD. By comparison, the state-of-the-art system in Gupta et al. (2010) proposed a face recognition algorithm based on geodesic and 3-D Euclidean distances between 10 automatically annotated anthropometric facial fiducial points ("Anthroface 3D"). The performance of Anthroface 3D was also evaluated on T3FRD with comparable size training, probe, and gallery sets. The highest performance reported by Gupta et al. (2010) is achieved in the recognition of neutral faces yielding $EER = 1.65\%$ and $AUC = 0.0014$ in a verification experiment and $RR1 = 97.3\%$ in an identification experiment. Our proposed iso-geodesic Procrustean contours based face recognition approach has significantly better performance than the algorithms in Gupta et al. (2010).

Zou et al. (2007) introduced "warping coefficients", a 3-D face recognition system based on warped range images. In this algorithm, a number of selected range images constitute a set of example faces, while another range image is selected as a "generic face". The generic face is then warped to match each of the example faces. Each such warp is specified by a vector of displacement values. In the feature extraction phase, when the algorithm is provided with a new range image, the generic face is warped to match it. The geometric transformation used in this warping can be approximated as a linear combination of example face warping vectors. The coefficients in the linear combination are used as features and passed to a Mahalanobis-distance based classifier. The "warping coefficients" achieved $EER = 2.5\%$ when evaluated using a subset of range images available in T3FRD. AUC and $RR1$ were not reported in Zou et al. (2007).

Mahoor and Abdel-Mottaleb's (2009) contour-based algorithm which recognizes faces by comparing their ridge lines
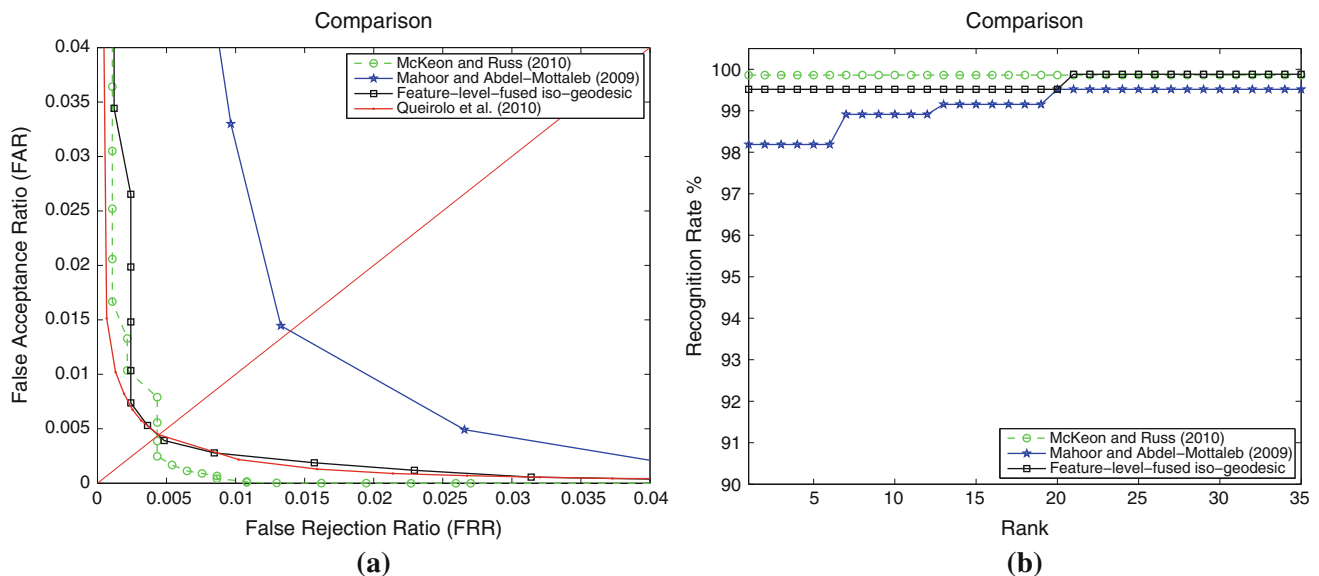

Fig. 15 Performance comparison between the proposed iso-geodesic contour-based algorithm and the state-of-the-art algorithms from literature: (**a**) ROC curves showing the verification accuracies (**b**) CMC curves showing the identification performance

using the ICP algorithm was evaluated on T3FRD with the same probe and gallery partitions. The ridge line algorithm, which is one of the leading contour-based algorithms evaluated on the FRGC database, achieves $EER = 1.39\%$ and $AUC = 0.0023$ in a verification experiment, and $RR1 = 98.19\%$ in an identification experiment.

Queirolo et al. (2010) proposed a 3-D face recognition algorithm founded on the "surface matching" and "region ensembles" concepts. In this framework, four regions are segmented on each face around automatically detected landmarks. When comparing two faces, their corresponding segmented regions are iteratively registered using a Simulated Annealing (SA) optimization that maximizes their Surface Interpenetration Measure (SIM). The SIM values corresponding to the matchings of four regions: circular and elliptical areas around the nose, forehead, and entire face are eventually summed up into a similarity score between two faces. Simulated Annealing is a stochastic algorithm for local search that when used in surface registration, is more likely than the conventional ICP to find the global optimum solution, but it is much slower than the ICP (Queirolo et al. 2010). Queirolo et al.'s (2010) face recognition algorithm, which is one of the leading performers on the FRGC database, was evaluated in verification mode with the exact same probe and gallery sets on T3FRD and yielded $EER = 0.46\%$ and $AUC = 0.0003$ (Table 6; Fig. 15) which is slightly outperformed by the EER and AUC achieved by the algorithm proposed in this work. However, Queirolo et al.'s (2010) algorithm had slightly better performance at lower FAR ranges. Similar to other iterative surface matching techniques (e.g. ICP), the main drawback of this algorithm is that an optimization-based comparison should be performed between the probe face and every face in the gallery that becomes computationally prohibitive when performing identification tasks on large databases.

Queirolo et al. (2010) used a computer with the following configuration: Linux O.S., Intel Pentium D 3.4GHz, cache of 2MB and 1GB of RAM and found the average execution time to be 4 seconds when comparing two faces using their proposed algorithm. As stated by Queirolo et al. (2010), Simulated Annealing's excessive time consumption limits the applicability of their proposed algorithm to verification application where the probe face is only compared to a single gallery image. In order to recognize a face among 103 subject in T3FRD, it would require $4 * 103$ seconds equal to 6 minutes and 52 seconds. As clearly stated by the authors in Queirolo et al. (2010), this algorithm is only viable for verification applications and is not applicable in identification applications where a face will be compared with hundreds of other faces. For example, identifying a probe face from among 103 registered subjects in T3FRD will require close to 7 minutes (Queirolo et al. 2010). By contrast, the algorithm

proposed in this work was able to execute the same identification task on average in 3 seconds while running on a computer with: Windows XP OS, Intel Core 2 CPU 2.00GHz, 2.0 GB of RAM. This 3 seconds includes: landmark detection, iso-geodesic contours extraction, pose invariant feature extraction, and comparison with 103 registered subjects using a Matlab implementation that was not optimized.

McKeon and Russ's (2010) 3-D Fisherface Region Ensembles method was also evaluated with the exact same probe and gallery sets on T3FRD. The proposed algorithm in McKeon and Russ (2010) combines a statistical learning approach with the region ensembles paradigm. In McKeon and Russ (2010), 22 regions are defined on the human face where a 3-D Fisherface (PCA followed by LDC) is applied to each region as the core statistical discriminator. The input features to each regional Fisherface are the concatenated (x, y, z) coordinates of all of the points in that region. In the training stage of this algorithm, sequential forward search (SFS) (Sharma 1995) is used to select the most discriminating regional Fisherfaces among the 22 candidates. The main drawback of the 3-D Fisherface Region Ensembles algorithm (McKeon and Russ 2010) compared to the algorithm proposed in this work is that McKeon and Russ's (2010) region selection requires a considerable number of training samples. McKeon et al. had to use the entire T3FRD sample set in addition to faces from FRGC 2.0 to train their algorithm. The performance of this algorithm is presented in Table 6 and Fig. 15. The 3-D Fisherface Region Ensembles method, which is currently among the top performing algorithms evaluated on the FRGC database, yielded $EER = 0.42\%$ and $AUC = 0.0007$ in a verification experiment, and $RR1 = 99.86\%$ in an identification experiment. This result is the best so far reported on T3FRD, however, it is achieved by incorporating all the T3FRD images at the training stage as compared to our approach, which produces comparable performance when trained with only 270 training images. Since the gallery and probe set used by McKeon et al. completely overlap with the training set, their reported results are biased.

Comparing the performances of other algorithms evaluated on T3FRD (Table 6; Fig. 15) with the performance of the proposed iso-geodesic contour-based algorithm, it is evident that defining appropriate contours, extracting pose invariant features directly from 3-D contours, carefully analyzing discriminative features around each landmark, and eventually merging an ensemble of face recognizers from different regions into a unified face recognizer yields a contour-based algorithm that outperforms other contour-based algorithms and that is competitive in terms of recognition performance as tested on T3FRD with a state-of-the-art algorithm that delivers top performance on T3FRD and FRGC, but which uses a much denser representation of the 3-D structure of the face.

7.5 Robustness Evaluations

In Sects. 7.1–7.3, the performance of the proposed face recognition algorithm was studied at different stages of the fusion hierarchy under the assumption that the fiducial points were automatically detected using range Gabor descriptors. The performance evaluations were conducted using a probe set containing both expressive and neutral faces. In the following subsections, we discuss the effects of automatic landmark detection on overall face recognition performance. We also evaluate the robustness of the proposed face recognition algorithms against facial expression changes. Finally, we assess the generalization capabilities of the proposed face recognition model by using test and training sets that are subject independent.

7.5.1 Sensitivity to Fiducial Detection Errors

In previous subsections, the performances of the algorithms derived from our proposed iso-geodesic face recognition models were studied at different levels of the hierarchy under the assumption that the fiducial points were automatically detected. In order to assess the effects of the "fiducial detection" errors on the performance of face recognition, the algorithms were re-evaluated using the same probe and gallery sets when the landmarks are pinpointed manually. Figure 16 and Table 7 summarize the face recognition results achieved in the absence of landmarking errors. Comparing the results in Tables 5 and 7, it is evident that most of the performance measures indicate a slight degradation by fiducial-scale face recognizers due to "automatic detection" landmarking errors.

Table 7 The observed EER, AUC, and RR1 values for the "Fiducial Scale Fusion" and the "Global Scale Fusion" with manually detected landmarks

Algorithm	EER (%)	AUC	RR1 (%)
LEIC	3.40	0.0075	91.67
REIC	3.76	0.0095	91.18
NT	1.21	0.0016	98.48
Match score-level	0.94	0.0009	99.03
Feature-level	0.36	0.0001	99.64

These performance declines eventually take a toll on the performance of ensemble face recognizers that combine information from different regions of the face. In the absence of landmarking errors, the feature-level fused face recognizer achieves $EER = 0.36\%$ and $AUC = 0.0001$ in the verification test, and a rank one recognition rate as high as 99.64% in the identification test. These results can be considered as an upper bound for the performance of the proposed algorithms. Although the performance of the proposed feature-level fused recognizer reduces when supplied with landmarking inaccuracies, this reduction is marginal.

7.5.2 Sensitivity to Facial Expression

In order to evaluate the robustness of the algorithms derived from our proposed iso-geodesic face recognition models against facial expression variations, an experiment was conducted in which subjects in T3FRD are enrolled in the gallery set by a neutral range image, and the probe set contains only expressive range images. The results of expressive
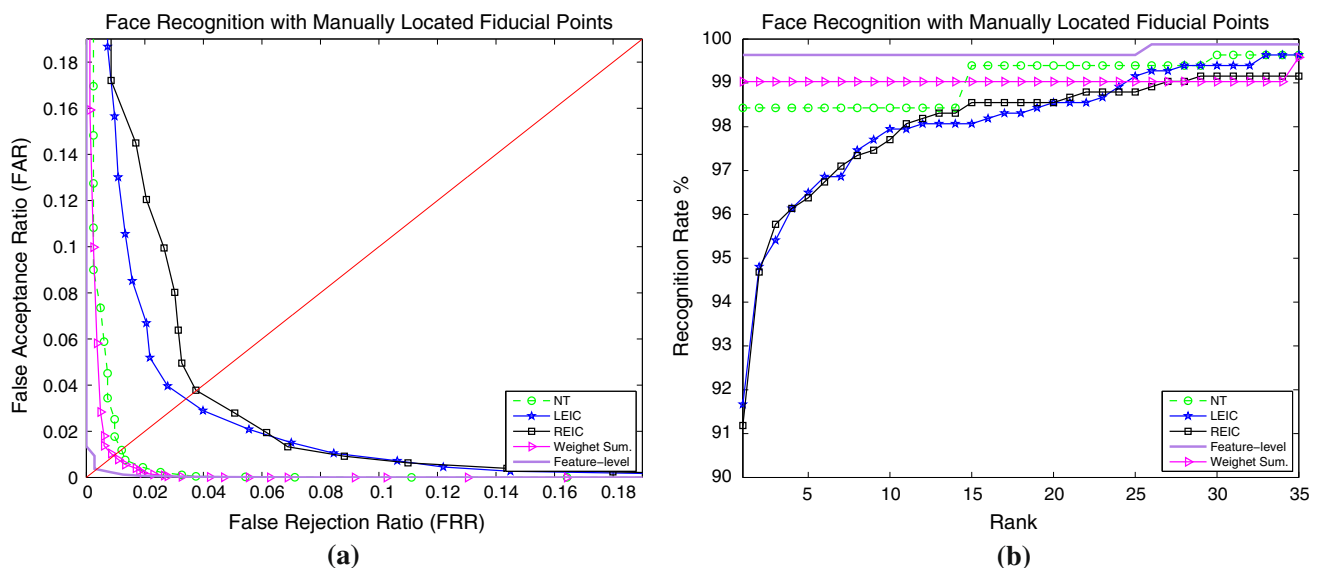

Fig. 16 Performance evaluation of the "Fiducial Scale Fusion" and the "Global Scale Fusion" with manually detected landmarks: (a) ROC curves showing the verification accuracies (b) CMC curves showing the identification performance
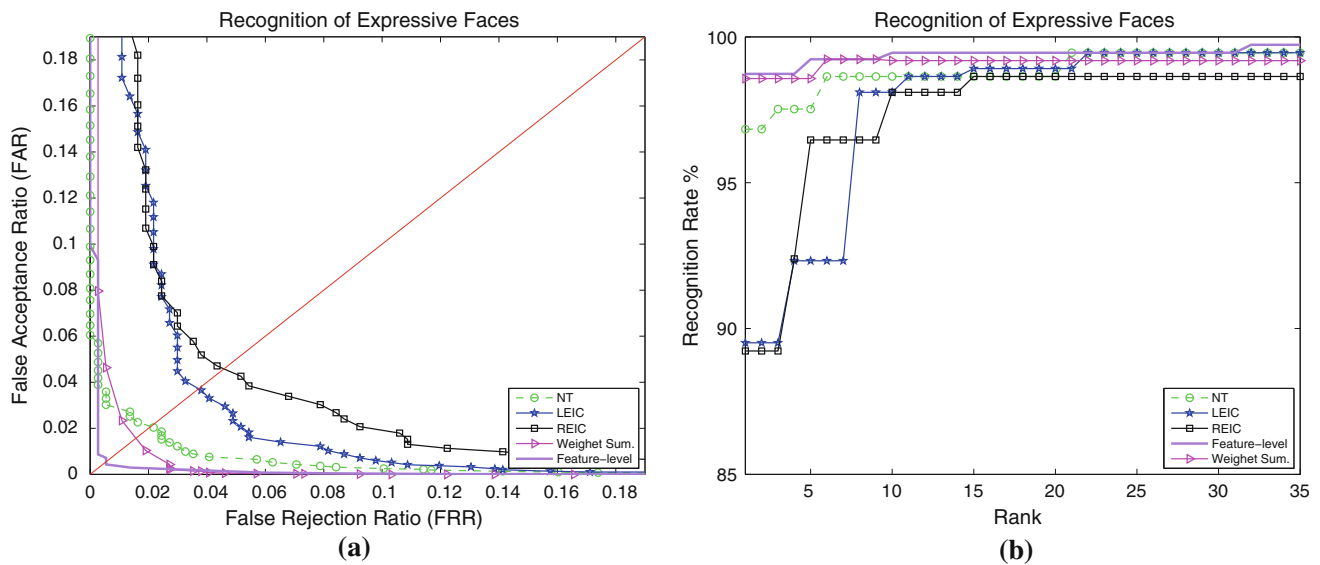
Fig. 17 Performance evaluation of the "Fiducial Scale Fusion" and the "Global Scale Fusion" in recognizing "expressive" faces: (**a**) ROC curves showing the verification accuracies (**b**) CMC curves showing the identification performance

Table 8 EER, AUC, and RR1 values for the "Fiducial Scale Fusion" and the "Global Scale Fusion" in recognizing "expressive" faces

Algorithm	EER (%)	AUC	RR1 (%)
LEIC	3.72	0.0098	89.51
REIC	4.58	0.0135	89.23
NT	2.08	0.0024	96.83
Match score-level	1.57	0.0013	98.57
Feature-level	0.54	0.0004	98.73

face recognition experiments are summarized in Fig. 17 and Table 8. Comparing the results in Tables 5 and 8 , it is evident that the fiducial-scale face recognizers perform less reliably when subjected to expressive faces. This performance slip is also evident in the performance of the final global-scale face recognizers as the observed verification equal error rate increase from $EER = 0.44\%$ to $EER = 0.54\%$ and the rank one recognition rate falls from $RR1 = 99.76\%$ to $RR1 = 98.73\%$.

Although the performance of the proposed iso-geodesic based face recognition system degrades when analyzing expressive faces, this reduction is marginal. The proposed face recognizer (at the global scale fusion) still achieves better or comparable performance in recognizing expressive faces than do other algorithms in recognizing combinations of expressive and neutral faces from the same database (Table 6). The robustness of the proposed algorithm against facial expression changes can be explained by the fact that this algorithm is founded on local features that are mostly extracted from rigid regions of the face that are less deformable with facial expression variations (nose region

and eye sockets). In addition, statistical learning techniques are employed to select the most discriminating and expression invariant features for each region and discard expression sensitive ones. Finally, the region ensemble approach is implemented using a hierarchical scheme that merge face recognizers from different regions of the face into a robust face recognition algorithm. Region ensemble approaches are known for being robust against facial expression changes and occlusion.

7.5.3 Generalization Capabilities

In order to assess the generalization capabilities of the proposed iso-geodesic contour-based face recognition models, performance evaluations were conducted on a "training-subject independent" testing set that does not contain any images from the 18 subjects present in the training phase (e.g. stepwise-LDA training). After removing training dependent subjects, the "training subject independent" testing set contains 300 range images from 85 subjects. The results of these generalization evaluation experiments are summarized in Fig. 18 and Table 9. Comparing the results in Tables 5 and 9, it is evident that the performances of the fiducial-scale face recognizers and eventual global-scale face recognizers show only a slight decline. These results confirm that the proposed training scheme is not biased towards subjects present in the training set.

8 Conclusion and Future Work

In this article we introduced a novel 3-D face recognition algorithm based on iso-geodesic contours and Procrustean
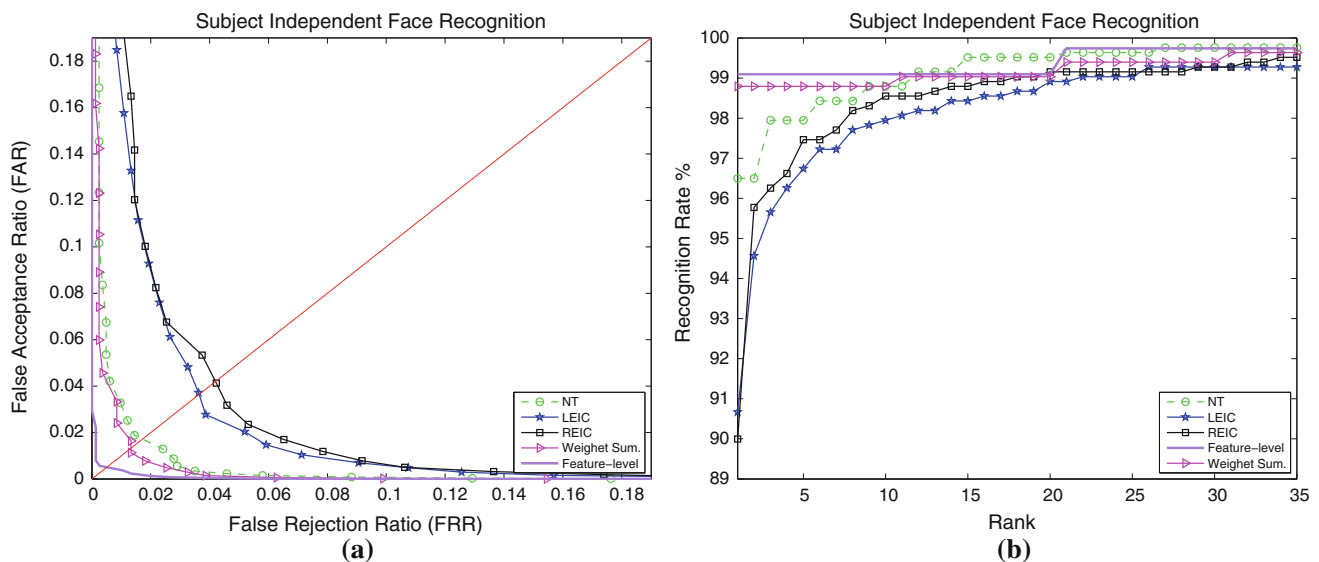
Fig. 18 Performance evaluation of the "Fiducial Scale Fusion" and the "Global Scale Fusion" evaluated using training-subject independent test set: (**a**) ROC curves showing the verification accuracies (**b**) CMC curves showing the identification performance

Table 9 EER, AUC, and RR1 values for the "Fiducial Scale Fusion" and the "Global Scale Fusion" evaluated using training-subject independent test set

Algorithm	EER (%)	AUC	RR1 (%)
LEIC	3.64	0.0095	90.66
REIC	4.20	0.0125	89.99
NT	1.72	0.0025	96.49
Match score-level	1.33	0.0011	98.79
Feature-level	0.50	0.0004	99.09

analysis around three automatically detected fiducials. One important characteristic of iso-geodesic contours is that they remain unchanged with rigid transformations of the face (pose invariance). Innovative feature sets were defined and extracted from the iso-geodesic contours in 3-D Euclidean space. By directly extracting features from 3-D contours rather than from their projections onto a reference plane, the important pose-invariance quality of the iso-geodesic contours remains intact. Various Procrustean analysis based feature sets collected around three fiducials at varying radii were hierarchically fused into a unified face recognition algorithm with boosted performance. Classification was performed by a 1NN classifier using Euclidean distance metric in LDA subspace and the results evaluated and compared in both verification and identification setups on the Texas 3-D Face Recognition Database containing 1196 range and colored texture images of expressive and neutral faces.

The evaluation results indicate that the integrated features increasingly become discriminative by moving from the raw features to higher stages of the fusion hierarchy. At the highest stage of the hierarchy two alternative fusion schemes, feature-level and match score-level, are employed to integrate the parallel NT, LEIC, and REIC face recognizers into unified face recognition systems. The evaluation results indicate that although both fusion schemes are successful in improving the recognition performance compared to constituting units, feature-level fusion achieves significantly better performances by having access to richer sources of information about the input patterns. Comparison of identification and verification accuracies achieved by the proposed algorithm with state-of-the-art algorithms evaluated on the same database highlights the effectiveness of the proposed iso-geodesic contours for representing the facial surface. We have shown that by using well defined yet simple features extracted from iso-geodesic contours, exceptionally competitive performances are achievable. Although our target application operates under quite specific conditions, we envision that feature-efficient contour-based algorithms such as the one described here could eventually be developed for the free-viewing scenario.

As a side note, The above mentioned hierarchical scheme was reimplemented by substituting 1NN classifiers using Euclidean distance metric with support vector machines (SVM) with radial base function (RBF) kernels. The SVM classifiers did not result in any significant improvement over the simple 1NN classifiers using Euclidean distance metric. In our view, this attests to the discriminative power of the iso-geodesic/Procrustean features deployed on high-information fiducial areas.

Finally, it is striking to observe that such highly competitive performances are obtained by utilizing a small fraction of the range data captured in iso-geodesic contours.

Saving facial contours instead of full range images can reduce the storage resources required for extremely large databases likely to emerge in the future. It should be noted that the current algorithm uses only 3 contours around each fiducial. Like any other face recognition algorithm, the performance of the proposed contour based face recognition algorithm will vary somewhat with the number of registered subjects. In order to counter this performance variation, the number of contours around the landmarks can be increased.

References

Bachelor of Science in Biometric Systems, West Virginia University. Retrieved from http://www.lcsee.cemr.wvu.edu/ugrad/degree-info.php?degree=bsbs.

Biometrics frequently asked questions (2006). Retrieved from http://www.biometrics.gov/Documents/FAQ.pdf

Berretti, S., Bimbo, A. D., & Pala, P. (2010). 3d face recognition using iso-geodesic stripes. *IEEE Transactions on Pattern Analysis and Machine Intelligence*, *32*(12), 2162–2177. doi:10.1109/TPAMI.2010.43.

Besl, P. J., & McKay, H. D. (1992). A method for registration of 3-D shapes. *IEEE Transactions on Pattern Analysis and Machine Intelligence*, *14*(2), 239–256.

Boehnen, C., Peters, T., & Flynn, P. (2009). 3D Signatures for Fast 3D Face Recognition. In M. Tistarelli & M. S. Nixon (Eds.), *Advances in Biometrics*, Lecture Notes in Computer Science (Vol. 5558, pp. 12–21). Berlin: Springer.

Bowyer, K., Chang, K., & Flynn, P. (2006). A survey of approaches and challenges in 3D and multi-modal 3D+2D face recognition. *Computer Vision and Image Understanding*, *101*(1), 1–15.

Bowyer, K. W., Chang, K., & Flynn, P. (January 2004). *A Survey Of 3D and Multi-Modal 3D+2D Face Recognition*. Tech. rep. Notre Dame Department of Computer Science and Engineering Technical Report

Bronstein, A. M., Bronstein, M. M., & Kimmel, R. (2005). Three-dimensional face recognition. *International Journal of Computer Vision*, *64*(1), 5–30.

Chang, K., Bowyer, K., & Flynn, P. (2003). Face recognition using 2D and 3D facial data. In *ACM Workshop on Multimodal User Authentication* (pp. 25–32).

Chua, C. S., Han, F., & Ho, Y. K. (2000) 3D human face recognition using point signature. In *Proceedings of the Fourth IEEE International Conference on Automatic Face and Gesture Recognition*, (Vol. 1, pp. 233–238)

Duda, R., Hart, P., & Stork, D. (2001). *Pattern classification*. New York: Wiley.

Due Trier, Ř., Jain, A. K., & Taxt, T. (1996). Feature extraction methods for character recognition-a survey. *Pattern recognition*, *29*(4), 641–662.

Egan, J. (1975). *Signal detection theory and ROC-analysis*. New York: Academic Press.

Faltemier, T., Bowyer, K., & Flynn, P. (2008). A region ensemble for 3-D face recognition. *IEEE Transactions on Information Forensics and Security*, *3*(1), 62–73.

Gokberk, B., Salah, A. A., & Akarun, L. (2005). Rank-Based Decision Fusion for 3D Shape-Based Face Recognition. *Lecture Notes in Computer Science*, *3546*, 1019.

Grother, P., Micheals, R., & Phillips, P. (2003). Face recognition vendor test 2002 performance metrics. In *Proceedings of 2nd International Conference on Audio-and Video-Based Biometric Person Authentication* (pp. 937–945).

Gupta, S., Castleman, K. C., Markey, M. K., & Bovik, A. C. (2010). Texas 3D Face Recognition Database. In *IEEE Southwest Symposium on Image Analysis and Interpretation, 2010 (SSIAI 2010)* (pp. 25–28).

Gupta, S., Markey, M., & Bovik, A. (2010). Anthropometric 3d face recognition. *International Journal of Computer Vision*, *90*, 331–349.

Gupta, S., Markey, M. K., & Bovik, A. C. (2007). Advances and challenges in 3D and 2D+3D human face recognition. In M. S. Corrigan (Ed.), *Pattern Recognition in Biology* (pp. 63–113). Nova Science Publishers, Inc.

Heseltine, T., Pears, N., & Austin, J. (2004). Three-dimensional face recognition: A fishersurface approach. In A. Campilho & M. Kamel (Eds.), *Image Analysis and Recognition* (pp. 684–691). Berlin: Springer.

Hesher, C., Srivastava, A., & Erlebacher, G. (2003). A novel technique for face recognition using range imaging. In *Proceedings Seventh International Symposium on Signal Processing and Its Applications, 2003* (Vol. 2, pp. 201–204). doi:10.1109/ISSPA.2003.1224850.

Hu, M. K. (1962). Visual pattern recognition by moment invariants. *IRE Transactions on Information Theory*, *8*(2), 179–187.

ICAO. (2004). NTWG. Biometrics Deployment of Machine Readable Travel Documents. Technical report. http://www.icao.int/mrtd

Jahanbin, S., Bovik, A. C., & Choi, H. (2008). Automated facial feature detection from portrait and range images. In *IEEE Southwest Symposium on Image Analysis and Interpretation, 2008 (SSIAI 2008)* (pp. 25–28).

Jahanbin, S., Choi, H., Liu, Y., & Bovik A. C. (2008). Three Dimensional Face Recognition Using Iso-Geodesic and Iso-Depth Curves. In *2nd IEEE International Conference on Biometrics: Theory, Applications and Systems, 2008 (BTAS 2008)* (pp. 1–6).

Kakadiaris, I., Passalis, G., Toderici, G., Murtuza, M., Lu, Y., & Theoharis, T. (2007). Three-dimensional face recognition in the presence of facial expressions: An annotated deformable model approach. *IEEE Transactions on Pattern Analysis and Machine Intelligence*, *29*(4), 640–649.

Kimmel, R., Sethian, J. (1998). *Computing geodesics on manifolds. Proceedings of National Academy Sciences* (pp. 8431–8435).

Kuhl, F. P., & Giardina, C. R. (1982). Elliptic Fourier features of a closed contour. *Computer graphics and image processing*, *18*(3), 236–258.

Latta, N. (2004). *US VISIT: Keeping Americas Doors Open and Our Nation Secure*. Washington, DC: Biometric Consortium.

Le Zou, S. C., Xiong, Z., Lu, M., & Castleman, K. R. (2007). 3-D face recognition based on warped example faces. *IEEE Transactions on Information Forensics and Security*, *2*(3), 513–528.

Lu, X., & Jain, A. K. (2005). Integrating Range and Texture Information for 3D Face Recognition. In *Proceedings of the Seventh IEEE Workshops on Application of Computer Vision (WACV/MOTION'05)* (Vol. 1, pp. 156–163). Washington, DC: IEEE Computer Society.

Lu, X., Jain, A. K., & Colbry, D. (2006). Matching 2.5 D face scans to 3D models. *IEEE Transactions on Pattern Analysis and Machine Intelligence*, *28*(1), 31–43.

Mahoor, M. H., & Abdel-Mottaleb, M. (2009). Face recognition based on 3d ridge images obtained from range data. *Pattern Recognition*, *42*(3), 445–451. doi:10.1016/j.patcog.2008.08.012. http://www.sciencedirect.com/science/article/B6V14-4T7F5JV-1/2/750012b09de8c1739c4bca5d009b3b57.

Maurer, T., Guigonis, D., Maslov, I., Pesenti, B., Tsaregorodtsev, A., West, D., & Medioni, G. (2005). Performance of Geometrix ActiveID 3D Face Recognition Engine on the FRGC Data. In *Computer Vision*

and Pattern Recognition, Workshop (p. 154). doi:10.1109/CVPR.2005.581.

McKeon, R., & Russ, T. (2010). Employing region ensembles in a statistical learning framework for robust 3D facial recognition. In *Fourth IEEE International Conference on Biometrics: Theory Applications and Systems (BTAS), 2010*, pp. 1–7. IEEE.

Milnor, J. (1963). *Morse theory*. Princeton, NJ: Princeton University Press.

Mokhtarian, F., & Mackworth, A. (1986). Scale-based description and recognition of planar curves and two-dimensional shapes. *IEEE transactions on pattern analysis and machine intelligence*, 8(1), 34–43.

Moon, H., & Phillips, P. J. (1998) *The FERET verification testing protocol for face recognition algorithms. Proceedings of the Third IEEE International Conference on Automatic Face and Gesture Recognition, 1998* (pp. 48–53).

Moorthy, A. K., Mittal, A., Jahanbin, S., Grauman, K., Bovik, A. C. (2010). 3D Facial Similarity: Automatic Assessment versus Perceptual Judgements. In *IEEE Fourth International Conference on Biometrics: Theory, Applications and Systems (BTAS, 2010)*.

Morgan, D., & Krouse, W. (2005). Biometric Identifiers and Border Security: 9/11 Commission Recommendations and Related, Issues.

Mpiperis, I., Malasiotis, S., & Strintzis, M. G. (2007). 3D face recognition by point signatures and iso-contours. In *Proceedings of the Fourth IASTED International Conference on Signal Processing, Pattern Recognition, and Applications* (pp. 328–332). Anaheim: ACTA Press.

Mpiperis, I., Malassiotis, S., & Strintzis, M. G. (2007). 3-D face recognition with the geodesic polar representation. *Information Forensics and Security, IEEE Transactions on*, 2(3), 537–547. doi:10.1109/TIFS.2007.902326.

Nagamine, T., Uemura, T., & Masuda, I. (1992). 3D facial image analysis for human identification. In *Conference A: Computer Vision and Applications, Proceedings of the 11th IAPR International Conference on Pattern Recognition, 1992* (Vol. 1, pp. 324–327). doi:10.1109/ICPR.1992.201567.

Peura, M., & Iivarinen, J. (1997). Efficiency of simple shape descriptors. In C. Arcelli, L. P. Cordella, & G. Sanniti di Baja (Eds.), *Aspects of Visual Form* (pp. 443–451). Singapore: World Scientific.

Peyré, G., & Cohen, L. D. (2006). Geodesic remeshing using front propagation. *International Journal of Computer Vision*, 69(1), 145–156.

Phillips, P., Scruggs, W., O'Toole, A., Flynn, P., Bowyer, K., Schott, C., et al. (2010). Frvt 2006 and ice 2006 large-scale experimental results. *IEEE Transactions on Pattern Analysis and Machine Intelligence*, 32(5), 831–846.

Phillips, P. J., Flynn, P. J., Scruggs, T., Bowyer, K. W., Chang, J., Hoffman, K., Marques, J., Min, J., & Worek, W. (2005). Overview of the face recognition grand challenge. In *IEEE Computer Society Conference on Computer Vision and Pattern Recognition 2005. CVPR 2005.* (Vol. 1, pp. 947–954).

Phillips, P. J., Grother, P. J., Micheals, R. J., Blackburn, D. M., Tabassi, E., & Bone, J. M. (2003). Face Recognition Vendor Test 2002. Tech. rep., National Institute of Standards and Technology. www.frvt.org.

Queirolo, C., Silva, L., Bellon, O., & Segundo, M. (2010). 3d face recognition using simulated annealing and the surface interpenetration measure. *IEEE Transactions on Pattern Analysis and Machine Intelligence*, 32(2), 206–219. doi:10.1109/TPAMI.2009.14.

Rosin, P. L. (2003). Measuring shape: ellipticity, rectangularity, and triangularity. *Machine Vision and Applications*, 14(3), 172–184.

Ross, A. A., Nandakumar, K., & Jain, A. K. (2006). *Handbook of multibiometrics*. Berlin: Springer.

Russ, T., Boehnen, C., & Peters, T. (2006). 3d face recognition using 3d alignment for pca. In *IEEE Computer Society Conference on Computer Vision and Pattern Recognition, 2006* (Vol. 2, pp. 1391–1398).

Samir, C., Srivastava, A., & Daoudi, M. (2006). Three-dimensional face recognition using shapes of facial curves. *IEEE Transactions on Pattern Analysis and Machine Intelligence*, 28(11), 1858–1863.

Sharma, S. (1995). *Applied multivariate techniques*. New York: Wiley.

Sun, Y., & Abidi, M. A. (2001). Surface matching by 3D point's fingerprint. In *Proceedings of the Eighth IEEE International Conference on Computer Vision, 2001 (ICCV 2001)* (Vol. 2, pp. 263–269). doi:10.1109/ICCV.2001.937634.